巴工業株式会社

走査型プローブ顕微鏡カタログ

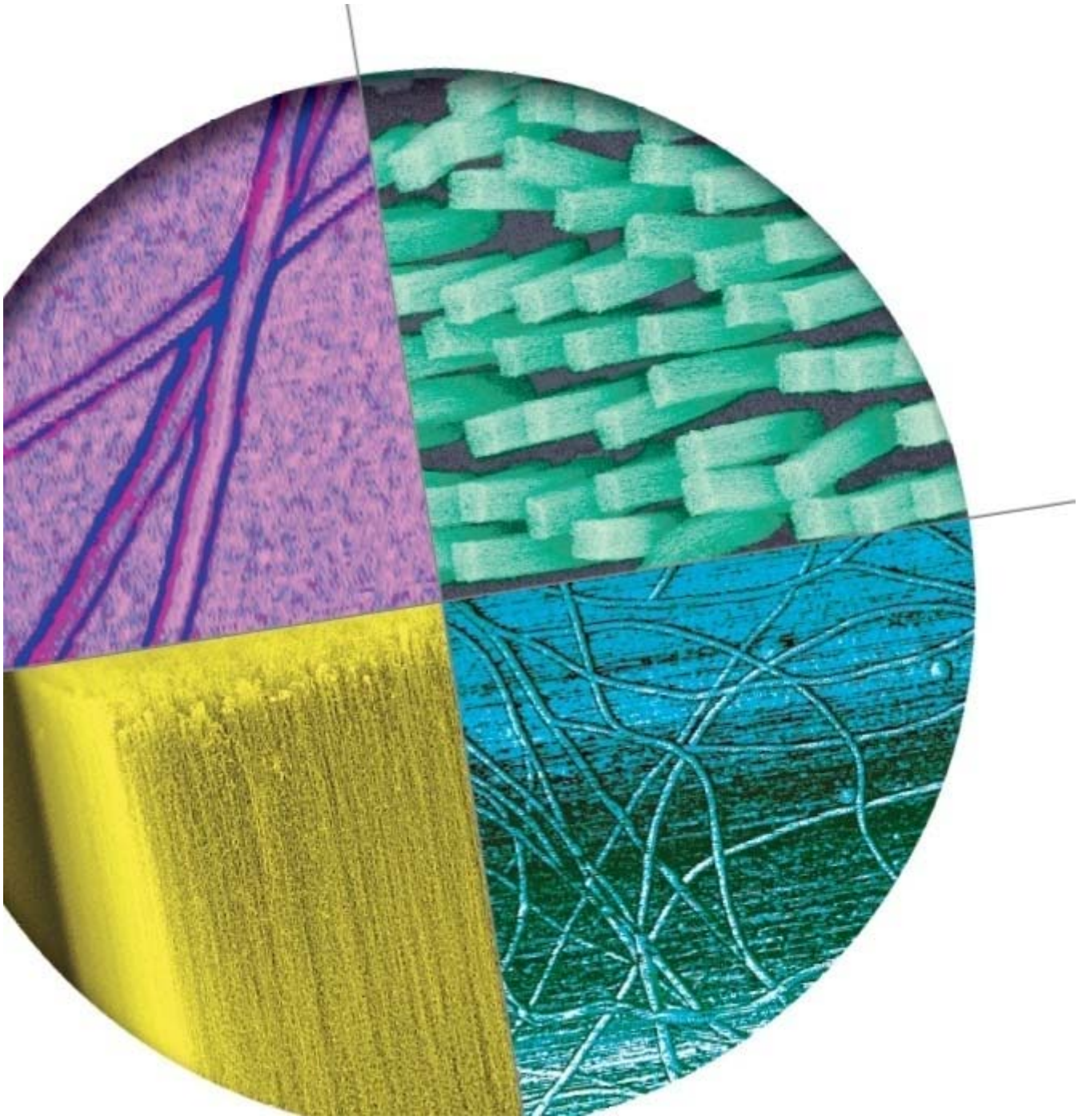

走査型プローブ顕微鏡（SPM）関連製品ラインナップ

巴工業は、世界各国の特徴のあるSPM用関連製品を紹介しています。
現在はイスラエル、ドイツ、オランダ、ブルガリア、USAからの製品を取り扱っております。

近接場光学顕微鏡(NSOM)
（イスラエル）

近接場光学の権威であるProf. Aaron Lewisが開発した、Nanonics社製NSOM/SPMの複合システムおよび、ガラス製NSOM/SPMプローブを取り扱っております。
メーカーです。顕微鏡を始め、様々な分析装置との連動が可能です。

SPM用プローブ

様々な会社の、特徴のあるプローブを取り扱っております。
現在、8社のプローブが販売可能です。

Q-Control/QFMモジュール
（ドイツ）

Munster大学からスピンオフして設立された、nanoAnalytics社製品を取り扱っております。こちらは世界で初めてQ-ControlをSPMに応用した製品になり、既存のSPMに組み込んで使用いたします。
Q-Control/QFMモジュールはカンチレバー共振周カーブのQ値コントロールと、CEモードでの周波数シフトイメージの取得が可能です。

熱測定(SThM)モジュール

Michigan大学からスピンオフして設立された、Picocal社製品を取り扱っております。こちらはポリイミド製熱測定プローブを用い、サンプルの温度分布をトポグラフィと同時に取得できます。
既存のSPMに組み込んで使用いたします。

MultiView NSOM/SPMシステム

特徴

NANONICS IMAGING Ltd.

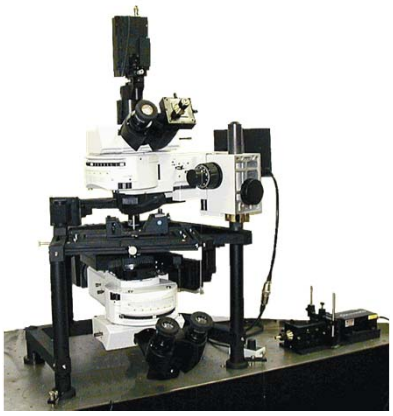

●先端が露出しているカンチレバー型光ファイバープローブ、上下方向で光学的にオープンな構造になっている3D Flat Scanner™を採用することにより、市販の光学顕微鏡（正立型、倒立型を問わず）へ容易に組み込むことが可能です。

●AFMと同じフィードバック機構を有するため、NSOM、SPMの同時測定、もしくは顕微光学測定、SPMの同時測定が可能です。
フィードバックには、従来の光テコ法とNanonics社独自のTuning Fork フィードバックの2種類から選択可能です。

●分光器、顕微ラマン装置、SEM、共焦点レーザー顕微鏡等の他の分析装置と組み合わせることが可能です。

●プローブは、Nanonics社製品以外にも、各種Siカンチレバーも使用可能です。

Nanonics社独自のテクノロジー

3D Flat Scanner™

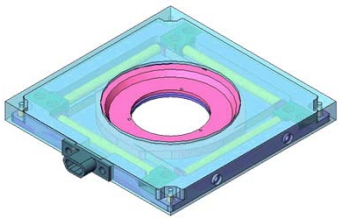

厚み7mmで、最大スキャンレンジがXYZ軸ともに70μmというスキャナーです。

ピエゾ素子の配置によりスキャナー中央に24mmの開口が開けられており、上下方向で光学的に オープンな構造になっています。また、厚みが7mmと薄いので、各種装置への組み込みも容易です。

カンチレバー型ガラスプローブ

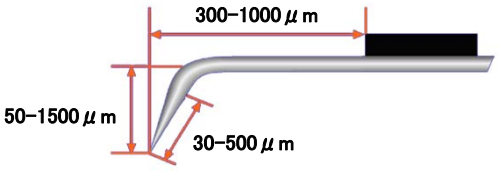

従来のカンチレバーとは異なり、先端が露出しており、またカンチレバーの Tip長が長いので、光学測定に影響を与えずにスキャンニングが可能です。

Nanonics社では、NSOMプローブ、AFMプローブ、Metal NanoWireプローブ、中空ナノピペット等特徴のあるプローブをご提供しています。

Normal Force Tuning Forkフィードバック

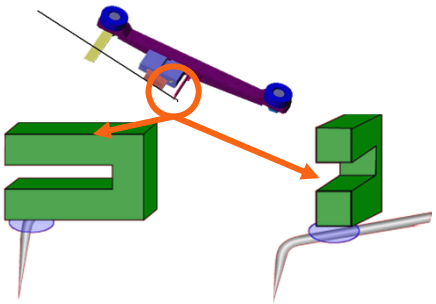

ガラスプローブに、高Q値のTuning Forkをとりつけ、Normal Forceフィードバックを行うものです。
これにより、光学的にオープンな構造を保ったまま、 プローブスキャニングが可能となりました。

特徴:
High Q factor
High Force Constant
No Jump to contact
Ultra soft contact
Optically free feedback
Amplitude/Phase Feedback

製品ラインナップ

NSOM/SPMシステム

MultiView4000 Multi Probe NSOM/SPMシステム

カンチレバー型光ファイバープローブの特長を最大限に生かした、画期的なモジュール型マルチプローブNSOM/SPMシステムです。ラインナップの中では、最も光学的にオープンな構造で、様々な光学測定との連動が容易です。

Tuning forkフィードバップローブ毎にスキャンモジュールが独立しており、 最大4本までのマルチプローブ測定が可能です。

それぞれのプローブとサンプル部は独立して制御可能です。スキャン モジュールは後から増設可能です。

基本動作モードはAC modeですが、オプションの光てこフィードバックにより、Contact modeへの対応も可能です（大気中/液中可）。

MultiVew2000 NSOM/SPMシステム

Tuning forkフィードバックを採用したことにより実現した、 プローブ/サンプルスキャニング方式のNSOMSPMシステムです。

プローブ側、サンプル側に3Dフラットスキャナーを2枚組み込んでおり、従来製品にくらべ、コンパクトな構造になっています。基本モードはAC mode（大気中/液中可）です。

MultiView1000 NSOM/SPMシステム

光テコフィードバックを採用した、サンプルスキャニング方式のNSOM/SPMシステムです。

基本モードはContact mode、AC mode（大気中/液中可）です。

CryoView2000 NSOM/SPMシステム

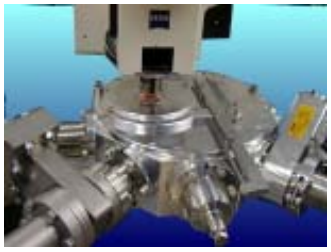

MultiView2000をベースにした、低温(10K)、高真空下でのNSOM/SPM/共焦点イメージングの同時測定が可能なシステムです。プローブ側、サンプル側に3Dフラットスキャナーを2枚組み込んでおり、プローブ/サンプルスキャニング方式になります。

基本モードはAC mode（大気中/真空中可）です。

NSOM/SPMプローブ

NSOMプローブ(光ファイバー)

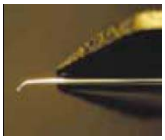
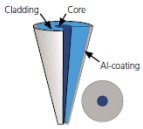

トポグラフィと近接場光イメージングが同時に可能な、カンチレバー型NSOMプローブです。開口径は50nm～300nmまで、50nmピッチで指定可能です。300nm以上の開口にも対応しています。

型番: CFN-XX　(XXは開口径)

ガラスAFMプローブ


ガラス製AFMプローブです。先端曲率半径は10nmからで、指定可能です。また導電コーティング(Cr/Au)も可能です。

型番: CAFP

Hollow Nano Pipette


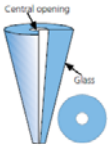

中空ガラスキャピラリを加工したナノオーダーのピペットです。ガスや液体を流すだけでなく、加工してNSOMプローブとして使用することもできます。先端開口径は20nmからです(NSOMは50nmから)

型番: CMP-XX　(XXは開口径)

TERSプローブ

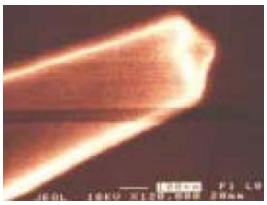

Hollow Nano Pipetteの先端に金属ナノ粒子を取り付けた、TERS用プローブです。

先端の金属はAuもしくはAgで、粒子径は50nmから作成可能です。

型番: CMP-TERS

Glass Insulated Nano Wireプローブ

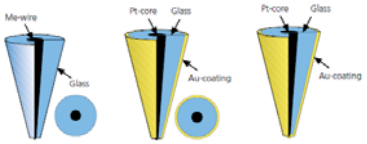

ガラスキャピラリの中にナノワイヤを組みこんだプローブです。用途に応じてCoaxial/電気化学用/熱電対が作成可能です。

型番: CM

複合測定アプリケーション

AFM/NSOM-SEM

広い範囲を高速に、高分解能で観察できるSEMと、3Dイメージングが可能な　AFMを組み合わせたアプリケ-ションです。MultiViewシステムはカンチレバー型ファイバープローブを用いてスキャン方向を変えることにより、SEMでは確認できない溝のサイドウォールのトポグラフィ像も取得できます。

AFM-Raman/TERS

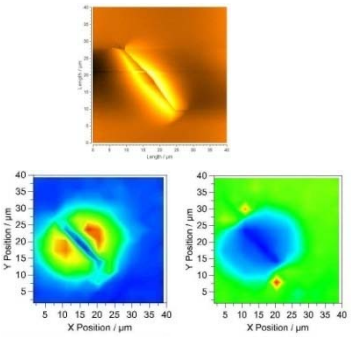

顕微ラマン分光器とMultiViewシリーズを組み合わせたアプリケーションです。AFMのフィードバック機構を用いてレンズーサンプル間距離をnmオーダーで一定に保つことにより、共焦点レ—ザ—顕微鏡と同様に空間分解能が向上し、 ラマン強度をサンプル表面形状の影響を受けずに正確に測定できます。

また、Nanonics社製Enhanced probeを用いることにより、TERS測定も可能です。

MultiView2000、MultiView4000がこのアプリケーションに適しています。

現在、Renishaw社製品、Jobin Yvon社製品、セキテクノトロン社製品に対応可能です。

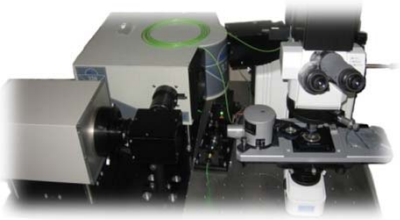

Fountain Pen Nanolithography™ Technology

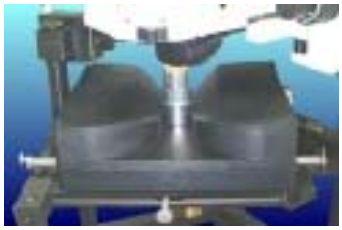

Nanonics社製カンチレバー型中空ナノピペットにたんぱく質等の分子を注入し、スキャンすることにより、基板上に分子をnmオーダーの精度で、デポジションさせることが可能です。たんぱく質の変わりに金属のナノパ-ティクルを使用したり、ガスもしくは液体を注入してナノエッチングを行うことも可能です。

屈折率測定アプリケーション

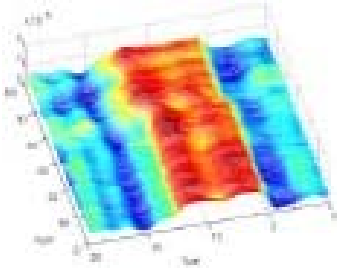

微分干渉顕微鏡とAFMフィードバックを組み合わせることにより、サンプルの屈折率分布が測定可能です。

屈折率の分解能は10^{-4}です（測定物の透明度に依存）。

また、測定物の反射率をNSOMで 高分解能に測定を行うことによっても屈折率分布が測定可能です。

MultiView シリーズ比較表

	MultiView1000	MultiView2000	MultiView4000
測定モード			
AFM	Contact mode AC mode	AC mode	AC mode Contact mode* （*光てこオプション時）
NSOM	Transmission Illumination mode Reflection Illumination mode Collection mode	Transmission Illumination mode Reflection Illumination mode Collection mode	Transmission Illumination mode Reflection Illumination mode Collection mode
液中測定	AFM/NSOMで可能	AFM/NSOMで可能	AFM/NSOMで可能
その他モード	MFM/導電測定/熱測定 /Nano fountain Pen/NanoIndentation	MFM/導電測定/熱測定 /Nano fountain Pen/NanoIndentation/ AFM-Raman/TERS	MFM/導電測定/熱測定 /Nano fountain Pen/NanoIndentation/ AFM-Raman/TERS
ヘッド仕様			
スキャン方法	サンプル	サンプル/プローブ	サンプル/プローブ
最大スキャン範囲	100μm(XYZ)	100μm(XYZ)	プローブ: 30 μm (XYZ) サンプル: 100 μm (XYZ)
スキャナー分解能	< 0.05 nm (Z) < 0.15 nm (XY) < 0.02 nm (XY) (low voltage mode時)	< 0.05 nm (Z) < 0.15 nm (XY) < 0.02 nm (XY) (low voltage mode時)	< 0.05 nm (Z) < 0.15 nm (XY) < 0.02 nm (XY) (low voltage mode時)
フィードバック方式	光てこ法式	Tuning Fork方式	Tuning Fork方式 光てこ方式(オプション)
顕微鏡仕様			
仕様可能な顕微鏡	市販の光学顕微鏡全般 （正立、倒立問わず）	市販の光学顕微鏡全般 （正立、倒立問わず）	市販の光学顕微鏡全般 （正立、倒立問わず）
必要な対物レンズWD	正立顕微鏡: 13mm （50 X 0.45NAが使用可） 倒立顕微鏡: 制限なし （油浸レンズ使用可）	正立顕微鏡: 7mm （100 X 0.75NAが使用可） 倒立顕微鏡: 制限なし （油浸レンズ使用可）	正立顕微鏡: 4.8mm （100 X 0.75NAが使用可） 倒立顕微鏡: 制限なし （油浸レンズ使用可）

SPM用プローブ

特徴

巴工業は、世界各国の特徴のあるSPM用プローブを紹介しています。
現在はドイツ、オランダ、ブルガリア、USAにある8社の製品を取り扱っており、これらのプローブは
市販されているほとんどのSPMで使用可能です。

プローブメーカーラインナップ

Innovative Solution Bulgaria 社(ブルガリア)	BudgetSensorsのブランド名で、安価で高品質なSPMプローブを提供しています。
team nanotec社（ドイツ）	IBMからスピンオフして設立された、世界で唯一プラズマエッチングでプローブを製作しているメーカーです。高精度のMEMS加工技術を持ち、電子線リソグラフィ用フォトマスク等のビジネスも展開しております。Tip形状はピラミッド形状ではなく、円錐形になります。また特注対応も可能です。
SmartTip社（オランダ）	Twente大学のSystems and Materials for Information Storage グループとの共同開発により誕生したメーカーです。学内のMESA+ナノテクノロジー研究所に隣接したMESA+ TechPark内に設立されています。磁気測定に特化しており、SmartCoat™と呼ばれるコーティングを施した高性能MFMプローブを提供しています。また、長寿命、高品質の化学修飾プローブも開発中で、2010年に販売開始予定です。。
Novascan社（USA）	化学修飾プローブ、コロイド（パーティクル）プローブを提供しているメーカーです。10年近い実績があります。
Microstar technologies社	1982年に設立され、Diamondプローブのみならず、Diamond Knife、Indenter、Diamond Firamentなど、Diamondを取り扱う経験の豊富なメーカーです。

各社とも特徴のあるプローブを取りそろえております。またカタログに載っていないメーカーもございますので、詳しくは弊社機能材料部までお問い合わせください。

BudgetSensors SPMプローブ

http://www.budgetsensors.com

BudgetSensors SPMプローブは、安価で高品質なプローブです。
Contact mode用、Intermittent contact mode用(高共振周波数/鄭共振周波数/低ばね定数)、Force Modulation用の3種類がベースになります。こちらに各種コーティング、Alignment grooveなどのオプションが選択できます。

主な仕様

- ・Tip形状　四面体
- ・Tip曲率半径　10nm以下
- ・Tip高さ　15um
- ・ハーフコーンアングル　20-25°（正面）
  25-30°（横）
- ・Rotated Tip　Tip前後が反転している形状で、SPMセット時に前後の角度がほぼ対称

Alignment grooves

プローブのホルダー部背面にアライメント用グルーブが形成されているプローブです。

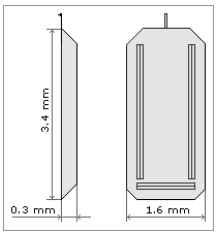

プローブラインナップ

プローブタイプ　*G: Alignment groove付き*

・Contact mode用プローブ
Contact/ContAl/ContAl-G

・Intermittent contact mode用プローブ
Tap300G/Tap300Al-G (高共振周波数)
Tap190G/Tap190Al-G (低共振周波数)
Tap150G/Tap150Al-G (低ばね定数)

・ Force Modulation用プローブ
Multi75G/Multi75Al/Multi75Al-G

・ MFMプローブ　MagneticMulti75G **New**

・シリコンナイトライドプロ-ブ　SiNi

・Special　AIO / AIO-TL New
一つのプローブに、Cont / Multi / Tap150 / Tap300 の4種類のレバーのついているプローブです。Tiplessも選択可能です。

各種コーティング

・反射コートティング(Al)
シリコンナイトライド以外のプローブで対応化

・導電コーティングプローブ(Pr/Cr)
ContG/Tap300G/Tap190G/Multi75Gに対応化

・金コートプローブ(全面及び背面)
ContG/Tap300G/Multi75G
Cont/Tap300/Multi75に対応化
全面コート(GB)及び背面コート(GD)より選択

・ DLCコーティング
ContG/Tap300G/Tap150G/Tap-190G/Multi75Gに対応化New

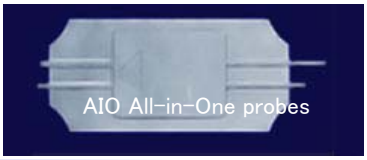

キャリブレーションスタンダード

Height Calibration Standard

正確なナノ・ミクロンオーダーの寸法測定を行うための、高品質の較正用サンプルです。

サンプルサイズ　5×5mm
ピッチサイズ:　10um(角柱)
　　5um(円形及びLine)
ステップハイト:　20nm(HS-20MG)
　　100nm(HS-100MG)
　　500nm(HS-500M)

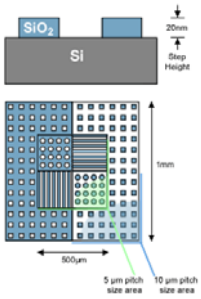

TipCheck

SPMプローブのTip先端の状態を評価できるサンプルです。

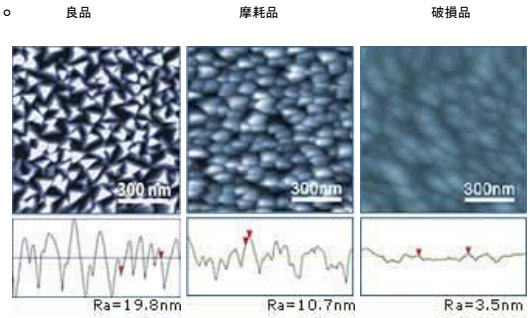

Mode	Type	Spring Constant (N/m, typ.)	Resonance Frequency (kHz, typ.)	Coating		Quantity	Cantilever
				Tip side	Back side		
Non-Contact / Intermittent Contact	Tap300	40	300	None	None	10/50/380	1 rectangular, Si
	Tap300AL			None	Al	10/50/380	
	Tap300GD			None	Au	10/50	
	Tap300GB			Au	Au	10/50	
	ElectriTap300			Cr/Pt	Cr/Pt	10/50	
	Tap300DLC			DLC	Al	10/50	
	Tap190	48	190	None	None	10/50/380	
	Tap190AL			None	Al	10/50/380	
	Tap190DLC			DLC	Al	10/50	
	Tap150	5	150	None	None	10/50/380	
	Tap150AL			None	Al	10/50/380	
	Tap150DLC			DLC	Al	10/50	
Force Modulation	Multi75	3	75	None	None	10/50/380	
	Multi75AL			None	Al	10/50/380	
	Multi75GD			None	Au	10/50	
	Multi75GB			Au	Au	10/50	
	ElectriMulti75			Cr/Pt	Cr/Pt	10/50	
	Multi75DLC			DLC	Al	10/50	
Contact	Contact	0.2	13	None	None	10/50/380	
	ContAL			None	Al	10/50/380	
	ContGD			None	Au	10/50	
	ContGB			Au	Au	10/50	
	ElectriCont			Cr/Pt	Cr/Pt	10/50	
	ContDLC			DLC	Al	10/50	
	SiNi	0.27/0.06	30/10	None	Cr/Au	30/100/300	2 trianguler. SiN
Special	MFM	3	75	Co Alloy	Al	10/50	1 rectangular, Si
	AIO	0.2/2.7/7.4/40	15/80/150/350	None	None	10/50	4 rectangular Si
	AIOAl				Al		
	AIO-TL				None		4 tipless rectangular Si
	AIOAl-TL				Al		

TEAM NANOTEC
MICRO- AND NANOFABRICATION TECHNOLOGY

team nanotec社 SPMプローブ

http://www.team-nanotec.de

プラズマエッチングを用いて、高品質のMEMSデバイス、リソグラフィ用フォトマスクと共にSPMプローブの製作/販売しています。

主な仕様

- Tip形状　円錐形
- フルコーンアングル　10°
- アスペクト比　1:5以上
- Tip曲率半径　10nm以下
- Tip高さ　15um
- 全品SEMによる出荷前検査を行うことにより、仕様を100%保証

カンチレバー標準寸法

l =125 (± 15) μm; w = 35 (±3) μm
Typ. stiffness: 40 N/m
Typ. res. frequency: 300 kHz

l= 225 (± 15) μm; w = 35 (± 3) μm
Typ. stiffness: 0.7 N/m; 3 N/m
Typ. res. frequency: 45 kHz ; 75 kHz

l = 450 (± 20) μm; w = 50 (± 3) μm
Typ.stiffness: 0.2 N/m
Typ. res .frequency: 15 kHz

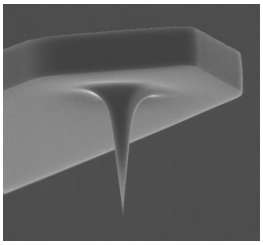

プローブラインナップ

SPMプローブ

ISC	標準プローブ、コーンアングルが全角で10°、アスペクト比 1:5以上
SS-ISC	先端曲率半径5nm以下の、高分解能測定用プローブ フルコーンアングル: < 5° (先端から150 nmまでの位置で)、Tip高さ: > 9 μm
EL-HAR5	メタルカーバイドをコーティングしたプローブ
HSC New	メタルカ-バイドもしくはSiNをコーティングした、導電測定、生体材料、ポリマー等のナノインデンテーションに適した、先端が半球状のプローブ(HemiSpherical Cone shaped tip)
LRCH New	広いスキャンレンジでの高さ測定、ナノインデンテーションに適した半球プローブ 曲率半径は250.500/750/1000nm、ばね定数は0.2～750N/mまで対応可
HR-MFM	Co-Alloyをコ-ティングした、高分解能MFMプローブ、コ-ティング厚は25nm/40nmより選択
HR-EFM	Ptをコ-ティングした、高分解能EFMプローブ、コーティング厚は25nm
Bio-SC New	Auをコ-ティングした、生体サンプル用プローブ
HR-SCC New	EBIDでSiカンチレバーにカーボンを成長させた、低価格な高分解能測定用カーボンプローブ 曲率半径3nm、Tip長さ>300nm
TNP 30Pt	Ptコートしたタングステンナノプローブ、先端曲率半径は30nm以下

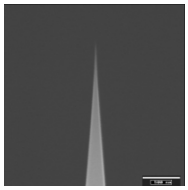
SS-ISC

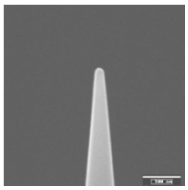
EL-HAR5

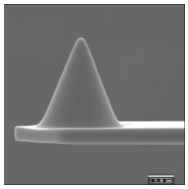
LRCH

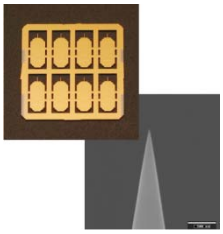
Bio-SC

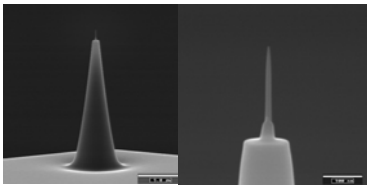
HR-SCC

TEAM NANOTEC
MICRO- AND NANOFABRICATION TECHNOLOGY

Cylindrical metrologyプローブ

溝の深さ測定に適したプローブです。同じ直径のまま摩耗して
いきますので、
生産環境での信頼性のある測定が可能です。導電カーボンコートも可能です。
Tip径は15nmから200nmまで取りそろえております。

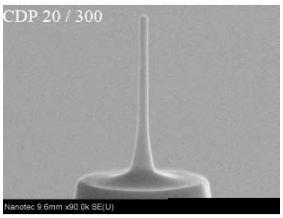

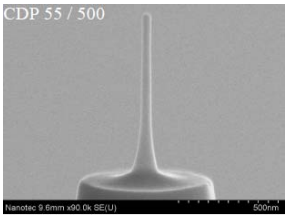

- 角度補正対応可能　　3°,10°,12°,13°
- Tip曲率半径　　10nm以下
- 基本カンチレバー寸法

　　l =125 (± 15) μm; w = 35 (±3) μm
　　Typ. stiffness: 40 N/m
　　Typ. res. frequency: 300 kHz

Critical Dimension(CD) プローブ

形状の3次元測定に適したプローブです。Tip先端にディスクが
ついた形状により、垂直方向の側壁も、たとえオーバーハングが
ついているものでもスキャンできます。
先端径は20nmから850nmまで取りそろえております。
Tip形状はRound、Triangular、Rectangular/Squareの3種類に
なります。

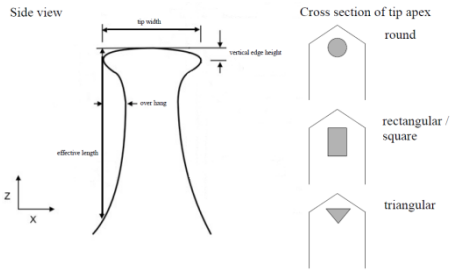

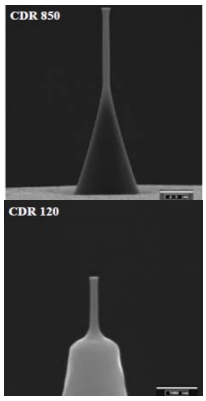

- 基本カンチレバー寸法

　　l =125 (± 15) μm; w = 35 (±3) μm
　　Typ. stiffness: 40 N/m
　　Typ. res. frequency: 300 kHz

特注プローブ

お客様の要望に合わせた特注プローブの制作が可能です。最小発注単位は30本～ですが、実績のある形状であれば5本単位からの販売の可能です。一度、お問い合わせください。

製作例 1

Super Sharp tip
on 1000 N/m cantilever)

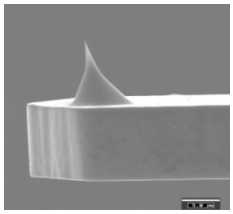

製作例 2

1.5 MHz cantilever for
high speed scanning

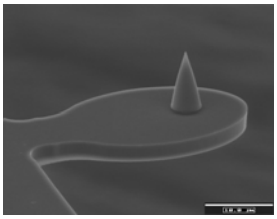

Tip Characterizer

プローブのTip形状を評価するための高精度に検査するためのSi製サンプルです。6×6mmのSi Chipに、88個のCellがあります。

IVPS	ピッチ測定、側壁測定用標サンプルです。
IVPS100	1cellに5ラインある、ピッチ測定、側壁測定用標サンプルです。
ISNE	鋭いnmオーダーのエッジを持った、Tip形状評価用サンプルです。
IFSR	オーバーハングしているエッジを持った、CDプローブ評価用サンプルです。

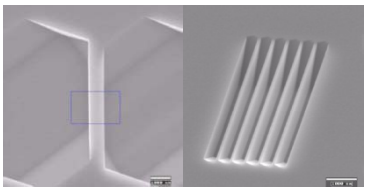

IVPS　　IVPS100

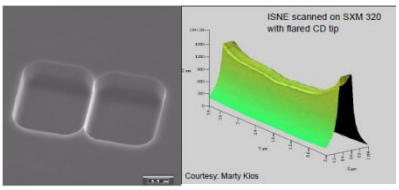

ISNE

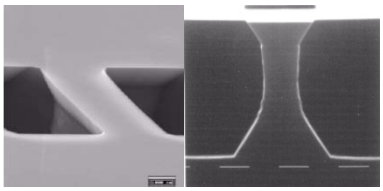

IFSR

SmartTip社　高分解能MFM用プローブ

http://smarttip.nl

磁気記録分野での学術研究・産業の両面にわたる経験に基づき，それぞれのお客様のアプリケーションに最適化したMFMプローブを提供しております．

SmartCoatとは

SmartCoatは、プローブTip部のピラミッドの一面のみに磁性コートを成膜する技術です。磁性コートはサンプルに対し垂直な面に施されます。

特長

- Tip部先端で明瞭で安定した磁性状態
- 印加磁場中の測定に適している
- 磁化方向がサンプルに対し垂直
- 先端曲率半径が従来のプローブに比べシャープ
- Tipからの磁気モーメントの低減
- カンチレバー部からの漏洩磁束による試料への影響を低減
- 硬質磁性コーティングプローブで軟質磁性材料の測定が可能

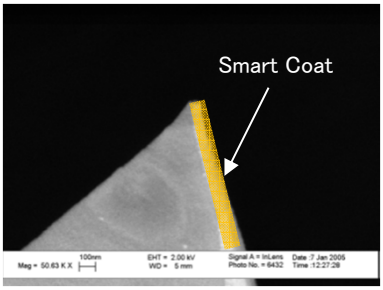

製品ラインナップ

SmartCoat スタンダードプローブ
SC-35-M/ SC-20-M /SC-10-M

市販のカンチレバーにSmartCoatを施した、標準タイプになります。

カンチレバータイプ:　FMR(Nanoworld製)
コーティング材料:　Ni-Co系
コーティング厚:　35nm/20nm/10nm
空間分解能:　25nm以上

SmartCoat Lpw Momentプローブ
SC-35-LM/ SC-20-LM /SC-10-LM

軟磁性材料の観察に適したコーティングの採用した低モーメントプローブです。

カンチレバータイプ:　FMR(Nanoworld製)
コーティング材料:　Co系
コーティング厚:　35nm/20nm/10nm
空間分解能:　25nm以上

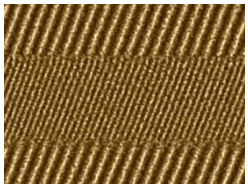

High density track in MP tape

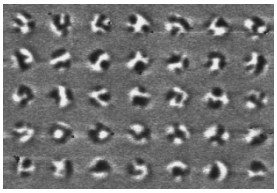

300 nm dot pattern, imaged with CantiClever high resolution probe

CIPTプローブ

CIPT測定用マイクロ12ポイントプローブ

CIPT装置用の低価格、長寿命、再現性の高いPin pitch distance、取り扱いが容易なセラミックマウント等の特徴をもったプローブです。

Available types / pin-spacing

Standard Type (007)
Pitch: 9.6, 9.3, 4.5, 3.0, 1.5, 1.5, 1.5, 1.5, 5.7, 12.4 μm

Narrow Type (004)
Pitch: 4.5, 3, 1.5, 1.5, 1.5, 1.5, 1.75, 2, 2.25, 2.5, 2.75 μm

Wide Type (005)
Pitch: 60, 24, 15, 6, 3, 3, 3, 3, 9, 12, 39 μm

General probe specs (all types)

Number of pins 12
Length of pins 10 (± 1.5) μm
Width of pins 600-750 nm
Pin thickness 1 μm
Coating Ti/Au
Coating thickness 5/100 (±10) nm

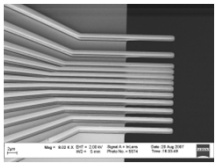

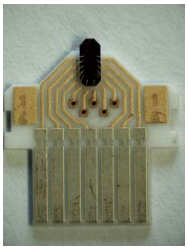

Novascan社　化学修飾 / パーティクルプローブ

http://www.novascan.com

化学修飾を施したプローブとカンチレバー先端にコロイド粒子をマウントしたパーティクルプローブを製造しています。

主な仕様

化学修飾プローブ

市販のAFMカンチレバーに化学修飾を施したプローブです。Novascan社製パーティクルプローブにも修飾可能です。

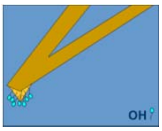

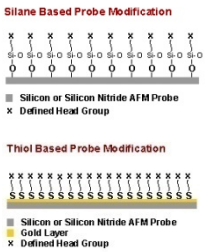

修飾可能な材質:

Alkanethiols:	COOH, CH3, NH2, OH, Succinimide
PEG Linkers:	PEG/COOH, PEG/NH2, PEG/Maleimide, PEG/Biotin
Silanes:	APTES
Others:	Biotin/Streptavidin/Neutravidin

パーティクルプローブ

tiplessカンチレバーに、コロイド球を接着したプローブです。

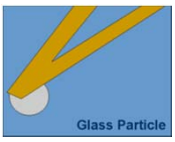

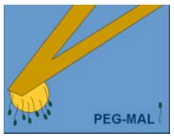

材質及びサイズ:

Borosilicate	2/5/10/12/20(μm)
SiO2	0.6/1/2.5/5(μm)
Polystyrene	1/4.5/10/25/45(μm)
Polyethylene	ご確認下さい
Tungsten	5/10(μm)

化学修飾/パーティクルプローブで選択可能なプローブのバネ定数及びコーティング

バネ定数	Si(N/m):	0.03/0.05/0.08/0.65/0.95/1.75/4.5/7.5/14
	SiN(N/m):	0.01/0.02/0.06/0.12/0.12/0.32/0.58
コーティング	Au / Nickel / Ag / Pt / Al / Chromium	

Potential Applications

Inter-molecular Force Measurement / Chemical Sensing and Detection / Adhesion Forces / Surface Mapping
Hydrophilic/Hydrophobic Interaction / Attractive/Repulsive Regimes / Unbinding Forces

MicaおよびGlass基板

SPMを始めとして、Confocal Microscopy、TIRF、Protein Binding Studies、Chemical Binding Studies、NSOMなどに用いるガラス/Mica基板です。

AFM グレードMica基板

AFM用基板として用いるMicaです。サイズは1×1cmで、1パッケージ50個入りです。
特注サイズ、Auコーティングを承っています。

化学修飾Mica/Glass基板

以下の材料を修飾したMicaおよびGlass基板です。

Amino Silanized (APTES)	Biotin terminated flexible PEG linker
Au coating with an OH surface	NH_3 terminated flexible PEG linker
Au coating with a CH_3 surface	Maleimide terminated flexible PEG linker
Au coating with COOH Surface	COOH terminated flexible PEG linker
Au coating with a succinimide surface	

Microstar technologies社Diamondプローブ

http://www.microstartech.com/

Si及びSapphire製tiplessカンチレバーに、単結晶Diamond tipを取り付けたプローブです

単結晶Diamond Tip

Tip形状は"3-SIDED PYRAMID"もしくは"Spike"から選択可能です。

3-SIDED PYRAMID
- Half Angle: 13° / 9° / 7°
- Tip高さ: 50-100um
  (300umまで対応可能)
- 先端曲率半径: <20nm※

※Half Angle 7° の場合は<5nm

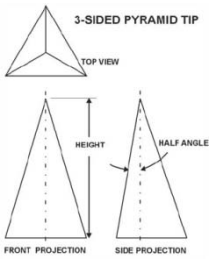

Spike(高アスペクト比)
- Tip幅 300nm
- Tip高さ: 1um
- 先端曲率半径: 3-4数nm

カンチレバー

カンチレバーは、SiもしくはSapphireより選択可能です。

Siカンチレバー: 以下の4種類より選択可
- Type M f=45kHz, L=225um, 1N/m
- Type N f=80kHz, L=225um, 4N/m
- Type P f=170kHz, L=225um, 40N/m
- Type Q f=320kHz, L=125um, 40N/m

Sapphireカンチレバー: 以下のパラメータを指定
- レバー長さ範囲: 200～1000um
- レバー厚み: 14～46um,
- ばね定数Type P f=170kHz, L=225um, 40N/m
- Type Q f=320kHz, L=125um, 40N/m

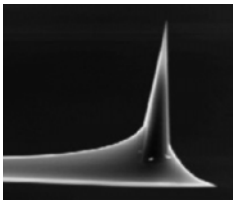

SEM Images of Diamond Tip on Silicon Cantilever

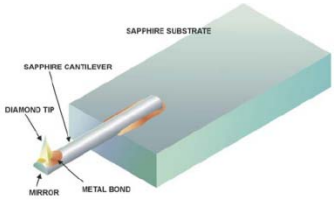

Sapphire Cantilever with Diamond Tip

その他仕様

- Conductive Diamond Tip(Sapphireカンチレバー)
  抵抗率=0.04Ω・m

- アクセサリー
  Veeco Multimode及びDimention/Bioscope用AFM module

ーDiamond Tipの再先鋭化サービス

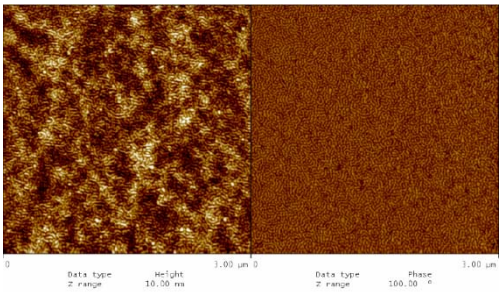

Tapping mode image of soft sample of triblock copolymer film using a diamond probe on silicon cantilever 4 N/m stiffness

HOPG

優れた性能を持つ高配向性結晶黒鉛です。
STM/AFM用標準試料、電極、薄膜成長用基板、黒鉛源、モノクロメータ等に用いられ、最近ではグラフェン形成にも用いられます。
以下の3種類のHOPGをご用意しております。

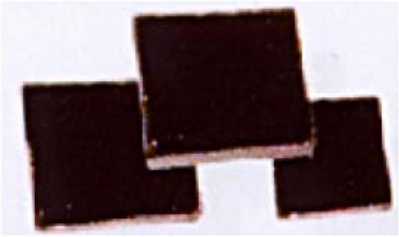

グレード	サイズ	モザイクスプレッド(°)
GRAS(ZYA)	12 X 12 X 1.5 mmt	0.4±0.1
GRBS(ZYB)	12 X 12 X 1.7 mmt	0.8±0.2
GRHS(ZYH)	12 X 12 X 2.0 mmt	3.5±1.5

nanoAnalytics　QFMモジュール

http://www.nanoanalytics.com

nanoAnalytics社製QFMモジュールは市販のSPMに組み込み、
FM modeでの動作とQ値制御を同時に可能とするモジュールです。
溶液中、大気中測定のどちらでも対応可能です。

概要

QFMモジュールは、AM(Amplitude Modulation) modeとFM(Frequency Modulation)でQ値制御をおこなうことのできるモジュールです。これにより、SPM プローブがサンプルに影響を与える力を最小化し、溶液中、大気中での柔らかいサンプルのイメージングを向上させます。

動作モード:

- FM-mode with CE(constant excitation)
- FM-mode with CE and Q-Control
- AM-mode ("tapping") with Q-Control

駆動周波数範囲： 7-25kHz/25-100kHz/100-500kHz

測定例

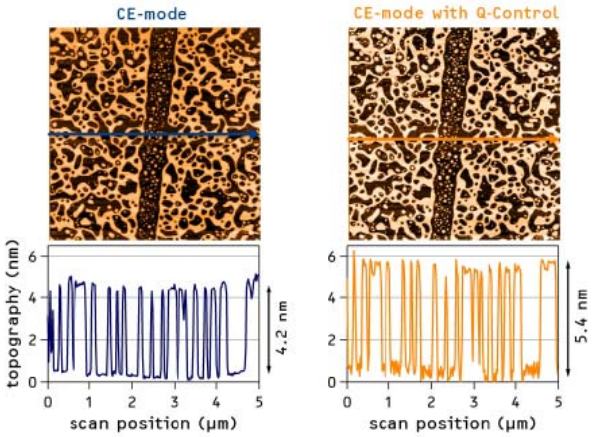

The top figure shows a Langmuir-Blodget film (DPPC) in liquid scanned in CE-mode. The observed height of the layer structure is significantly larger in case of imaging with Q-Control.
[D. Ebeling, H. Hölscher, B. Anczykowski, Appl. Phys. Lett. 89, 203511 (2006)]

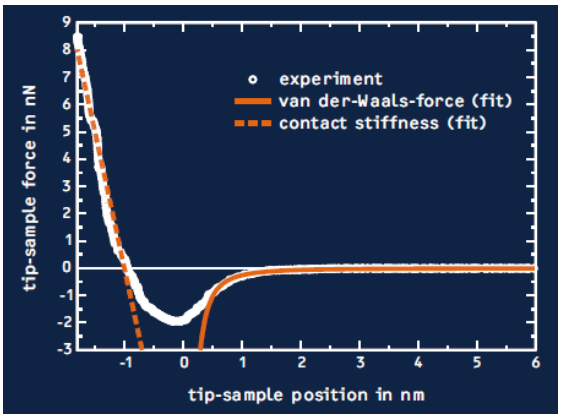

A tip–sample force curve obtained with a silicon cantilever on an untreated silicon wafer (symbols). The right part of the curve is fitted with a force law describing long-range van-der-Waals forces (solid line). The repulsive part on the left increases nearly linear with a contact stiffness of 10 N/m (dashed line)
[H. Hölscher, B. Anczykowksi, Surf. Sci. 579, 21 (2005)]

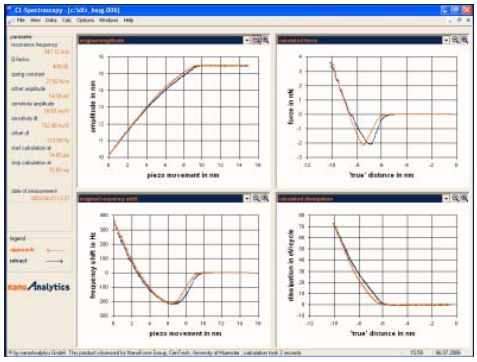

In FM-mode with constant-excitation (CE-mode) conservative and and dissipative tip-sample interactions can be directly determined. The customized analysis software which is provided with the QFM-Module enables the user to easily quantify tip-sample forces.
[H. Hölscher, B. Gotsmann, A. Schirmeisen, Phys. Rev. B 68, 153401 (2003)]

MICROMACHINED THERMAL PROBE AND MODULE

FOR HIGH RESOLUTION THERMAL DIAGNOSTICS BY

PicoCAL

- Scanning thermal microscopy is an add-on option to the standard AFM system.
- The key element of the SThM is a micromachined thermal probe.
- PicoCal has developed a thermal control circuit unit, ST 50™, that transmits temperature contrast imaging.
- Temperature and topographic data can be gathered simultaneously.
- The ST 50™ thermal unit is easy to interface with an AFM/SPM.
- The probe is interfaced with the module and the module cables plug into the AFM controller.
- The ST50 provides thermal conductivity analysis with a gain of up to x 10,000.
- The probe signal is connected to the INPUT of the module using a BNC cable and the OUTPUT of the module to the AFM controller.

THERMAL CONDUCTANCE IMAGING

High Resolution Latent Image Pattern Polymide probe was adequate for mapping 70 nm exposed but undeveloped contact pattern. *Undeveloped Photoresist-UV113 Thickness: 400 nm, 4 / 400 nm = 1%,* Scan condition: 0.75 µm/s; 400 lines Sample provided by Dr. Leo Ocola, Bell Labs.
Li et al. Hilton Head, 2002

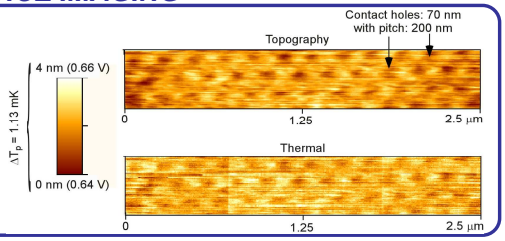

HOT SPOTS

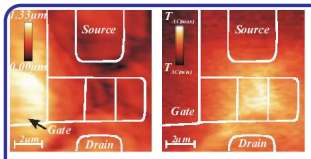

Hot-spot detection: a)Topo., b) thermal.

Images reveal that the highest amplitude of thermal waves generated by an operating *n*MOSFET is always located at a region close to the drain area. *Hendarto et al. IRPS – IEEE 2005*

SUBSURFACE IMAGING OF Cu WIRES

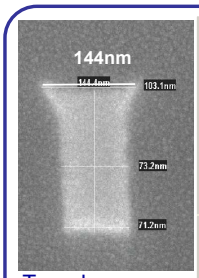

Trench preparation before Cu deposition. (SEMATECH sample)

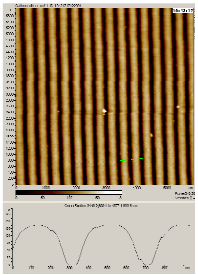

Topographical image of Cu lines under a natural oxide (125 nm thick, 300nm wide).

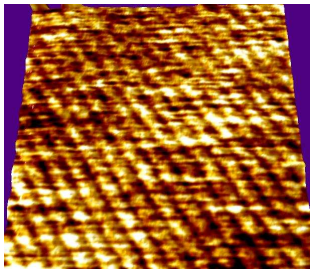

2 µm

Overlay of thermal on topo. image shows subsurface variations. This is not observable with a topo. scan.
6x6 µ m area
1 Hz scan rate
Scan conditions: 12 mA, probe 26 Ω
Gaitas, Micorscopy and Analysis, 2006

200nm subsurface variations of Cu lines not visible topographically

SUBSURFACE DETECTION

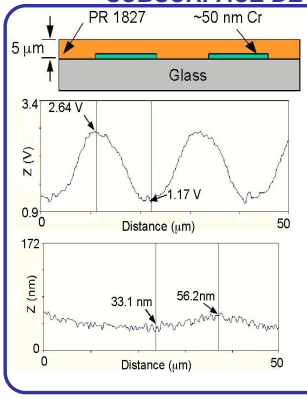

(above) A thin layer of chromium detected through 5 µm of photoresist, not possible using an AFM (below). *Lee & Gianchandani, Review of Scientific Instruments, Vol. 75, No. 5, 2004*

PROBE CHARACTERISTICS

Performance	PicoCal Probe
Tip Diameter	< 100 nm
Topographical Resolution	< 1 nm
Tip Temperature Resolution	< 10 mK
Spring Constant	< 0.1 N/m
Detectable Thermal Conductance Change	< 3 pW/K

- Temperature Range: 0 - 250 C
- Nominal Resistance: 20-40 Ohm
- Temperature coefficient of resistance 488ppm/C ±10%.
- Material: Bolometer made of Cr/Au for the tip and lead sandwiched
- between two layers of polyimide, forming a cantilever.
- 250 µm (length) × 50 µm (width) × 3 µm (thickness)
- Resonance frequency: 50 kHz

BIOLOGICAL SAMPLES: HELA CELLS

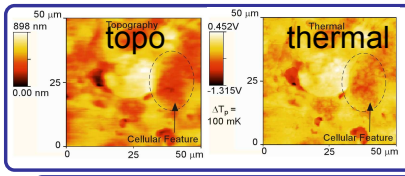

Thermal image provides sub-surface information
Li et al. Hilton Head, 2002

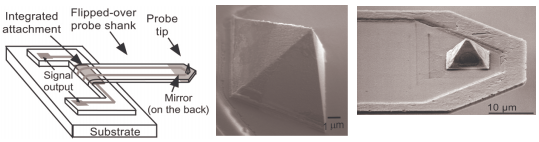

Scanning Thermal Probe

ST50 Module

info@picocal.com
www.picocal.com
(734) 972-9348, 913-2608

Polyimide Probes for Contact-Mode SPM Subsurface Thermal Imaging Applications

Angelo Gaitas, PicoCal Inc. and University of Michigan, Ann Arbor, USA

BIOGRAPHY

Angelo Gaitas is the president and CEO of PicoCal Inc. and a research associate in the Electrical Engineering and Computer Science Department at the University of Michigan, Ann Arbor. He received an MBA from the University of Wisconsin, Madison, and an MS in solid-state physics from the University of London. His research interests span a variety of scanning probe microscope techniques for manufacturing applications.

ABSTRACT

This article describes the results obtained with a surface micromachined probe for scanning thermal microscopy. The probe uses polyimide as the structural material and an embedded thin-film metal resistor as the sensing element. The typical dimensions of a probe are 250 µm in length, 50 µm in width, and 3-10 µm in thickness. The probe has measured spring constant less than 0.1 N m^{-1}, and about 40 Ω nominal resistance. It offers a tip diameter of 100 nm. The probe was used to map the spatial variation in thermal conductance of various test samples. Surface and subsurface characteristics were observed.

KEYWORDS

scanning probe microscopy, atomic force microscopy, scanning thermal microscopy, microthermal analysis, polymers, failure analysis, nanoscience, nanotechnology

ACKNOWLEDGEMENTS

The author would like to thank Prof. Yogesh Gianchandani, Dr Song Xu and Dr Shamus McNamara for their valuable contributions to this paper, and Sematech for providing samples.

AUTHOR DETAILS

Angelo Gaitas,
PicoCal Inc.,
PO Box 131490,
Ann Arbor, MI 48113-1490, USA
Tel: +1 734 913 2608
Email: angelo@picocal.com

Microscopy and Analysis 20(2):S11-S14 (UK), 2006

INTRODUCTION

Thermal measurements at the nanometer scale are of both scientific and industrial interest. Over the past decade, scanning microscopy using thermally sensitive probes has been used in a variety of applications. For instance, scanning thermal microscopy (SThM) has been used for ultralarge-scale integration (ULSI) lithography research and cellular diagnostics in biochemistry [1-3], detecting parameters such as phase changes in polymer blends [4], Joule heating [5], for measuring material variations in semiconductor devices [6], and subsurface imaging of metal particles [4]. Furthermore, SThM has been used to perform near-field photothermal microspectroscopy [8]. Finally, it has been used for data storage and many other applications [9-11].

Various thermal probes have been developed since the invention of scanning thermal microscopy by Williams and Wickramasinghe in 1986 [12]. These probes are generally made from thin dielectric films on a silicon substrate and use a metal or semiconductor film bolometer to sense the tip temperature. Other approaches, using more involved micromachining methods, have also been reported [13]. In a bolometer probe, such as the one used in this study, the resistor is used as a local heater and the fractional change in probe resistance is used to detect the temperature and/or the thermal conductance of the sample [14].

Thermal probes are used to map the spatial variation in thermal conductance of various test samples whose subsurface variations are not detectable topographically. This article presents a preliminary study of subsurface imaging on copper wires using a polyimide thermal probe. The ultimate goal of this effort is to address the semiconductor industry's challenge to develop non-destructive in-line viewing of copper voids. The use of SThM holds significant promise to detect defects such as voids in copper lines in advanced complementary metal oxide semiconductor (CMOS) processes. Since copper interconnects are common in advanced CMOS devices, it is vital for the semiconductor industry to obtain timely information about the quality of the copper electroplating process and related steps.

The use of non-electrical inspection methods for copper electroplating has several limitations. Because copper is opaque, optical inspection methods are difficult. In addition, since most of these failures occur on the interior of the copper trace, their detection is also difficult with topographic measurement methods using an atomic force microscope (AFM) or scanning electron microscope (SEM). While electrical methods are accurate, they require at least two points of contact and special geometries that permit access to both ends of the trace to be measured; this access is usually not available without special test structures. Another option, thermal measurement methods, can potentially overcome the problems posed by optical, AFM, SEM or electrical test methods. Such techniques measure the interior of the copper trace, enabling the non-destructive localized detection of voids in the copper. Thermal measurements require only a single point of contact and permit inspection of all the copper traces, regardless of geometry. Vias may be inspected because the barrier layer or remaining dielectric material have a much higher thermal resistance compared to copper.

Scanning thermal probes fabricated by six- to seven-mask surface micromachining processes using polyimide as the cantilever

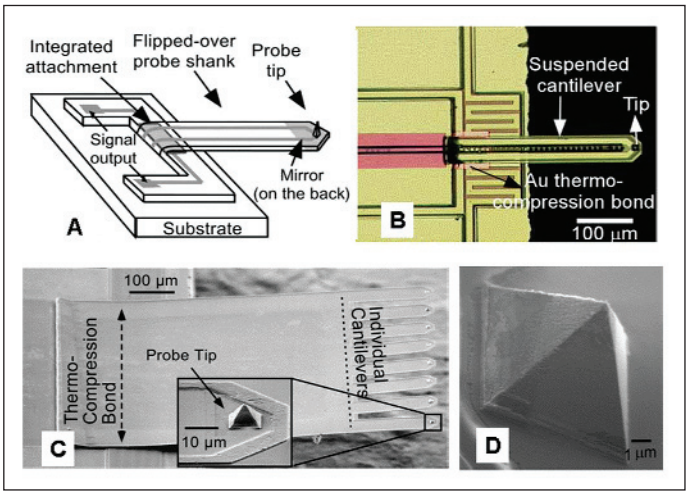

Figure 1:
(A) Schematic of the probe die including the probe cantilever and tip. Reprinted from [1] with permission.
(B) Scanning electron microscope image of the probe. Reprinted from [1] with permission.
(C) SEM image of an eight-probe array . Reprinted from [20] with permission.
(D) SEM image of a tip.

material have been previously reported [1,2,14,15]. These probes have been used for temperature mapping and subsurface imaging [15], for microcalorimetry applications to measure the glass transition temperature in a photoresist [1,2,14], and for maskless submicrometer thermochemical patterning of photoresists [16]. Hendatro *et al*. [17] used the probes for the detection of hot-spots in integrated circuits (IC) revealing that the highest amplitude of thermal waves generated by an operating nMOSFET (n-type metal-oxide semiconductor field-effect transistor) is located at a region close to the drain area. Basu *et al*. [19] have been using the probes for microfluidics-related work, namely for high-speed liquid pumping, mixing and particle entrapment in thin layers of oil and water. The probes have been arrayed into a multi-probe system for higher throughput large area scanning [20]. An eight-probe array, such as the one in Figure 1C, has been used to produce composite thermal images of various commercial ICs. Finally, the probes were used for high-speed contact mode topography achieving rates of 48 Hz (1.47 mm s^{-1}) and for lateral force scans, suggesting that polyimide is a more suitable structural material for cantilevers used in lateral force measurements [21].

MATERIALS AND METHODS

Structure and fabrication

The structure of the polyimide probe is shown in Figure 1. The probe tip diameter used was less than 100 nm but the probe tip can be further reduced to below 50 nm with oxide sharpening. The probe had a topographical resolution of <1 nm and a spring constant of <0.1 N m^{-1}. The tip height was 8 µm, and the cantilever's dimensions were 250 µm × 50 µm × 3 µm. The cantilever material was polyimide with an embedded thin wire of Cr/Au, which also served as a sensing element. The tip was also made of Cr/Au. The probe had spatial resolution of less than 100 nm. Thermal conductance changes of the order of 3 pW K^{-1} have been measured. A comparison with a Wollaston wire thermal probe is presented in Table 1.

The probes were microfabricated in a seven-masking step sequence. Initially, a mold for the tip was created by anisotropic wet etching on a Si(100) substrate. Then a sacrificial layer was deposited and patterned, followed by the lower polyimide and the metals. Later, the second polyimide layer was deposited and patterned, followed by a gold layer, which was used for thermocompression bonding and served as a mirror. Finally, the probe was released, flipped over, and held in place by a thermocompression bond.

Interface circuit and setup

There are many methods by which a thermal probe may be utilized. It can be operated in a passive manner whereby the tip temperature attains the localized sample temperature. In order to map the thermal conductance of samples, the probe is typically operated at an elevated temperature. The varying heat loss is monitored by its effect on the tip through the sample to the chuck below, which is held at room temperature. The simplest interface circuit operates in approximately constant power mode where an open-loop interface circuit is used to gauge the probe resistance change (thermal conductance change), which can be calculated from the output voltage change. The interface circuit includes a Wheatstone bridge, gain stages, and filters to reduce noise. The output voltage is plotted for the thermal image. In the case of thermal conductance contrast mapping, the change in probe resistance is proportional to the change in output voltage. The supplied power change is equal to the conductive heat loss between the tip and sample, which is proportional to the change in the thermal conductance of the sample. Thus the change in output voltage represents the thermal conductance contrast of the sample [1].

Alternatively, the scanning thermal probe may be operated at a constant tip temperature and the power required to keep the temperature constant is measured (closed-loop mode – feedback required). This method permits contrast imaging and thermal conductivity measurements to be performed. When the Wheatstone bridge comes out of balance, an instrumentation amplifier amplifies the change in voltage. Subsequently, the change in voltage is fed into a proportional-integral (PI) controller that provides a compensation current to keep the bridge balanced. The average probe temperature increases or decreases with the compensation power, so that the probe resistance is adjusted by a compensation current through the PI controller until the change in voltage is zero. By increasing the temperature control resistance, the probe resistance is also increased.

An AC thermal dither may be applied to the probe to improve thermal resolution or to perform thermal capacitance measurements. The thermal resolution is improved by filtering the signal through a bandpass filter to reduce the noise level. Since the thermal wave generated is an evanescent wave, the AC thermal dither may be used to control the effective probe depth. Higher frequencies of operation reduce the effective probe depth.

AFM systems for thermal probes

The probes may be operated with an AFM system. The thermal information from the probes was fed to a circuit module such as the one described above, which in return interfaced with an AFM controller (Figure 2A). In these measurments the probe was operated in contact mode by scanning a thermal probe tip across the sample and making measurements at discrete points. Thermal probes operated in contact mode show improved performance. By contrast, operation in a tapping or non-contact mode has several disadvantages. First, the temperature sensitivity of the probe is compromised because of the large thermal

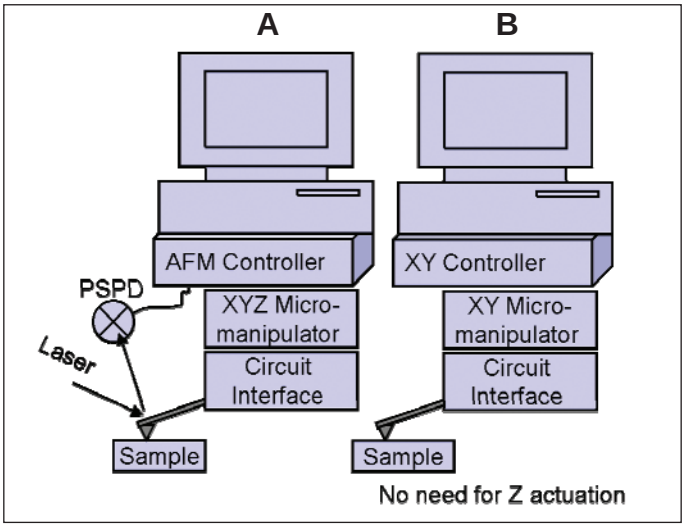

Figure 2:
Comparison of original AFM imaging mode (A) and a simpler system for thermal measurements in which Z-axis actuation is eliminated (B).

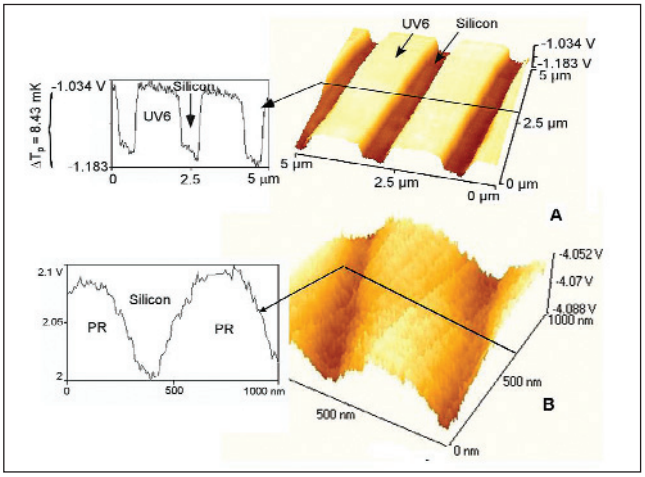

Figure 3:
AFM images taken without Z-direction feedback.
(A) Scans of a developed UV6 photoresist. The photoresist pattern is 350-nm thick and 500-nm wide. Reprinted from [1] with permission.
(B) Map of thermal conductance of a developed PMMA photoresist on a 4-inch silicon wafer. The photoresist pattern was 240-nm thick and 200-nm wide with a pitch of 400 nm. Reprinted from [22] with permission.

resistance of the air gap. Second, spatial resolution is reduced because the effective sensing area is enlarged as the distance between the sensor and the sample increases. Third, high stiffness in the probe is required which may cause damage to soft samples. The use of polyimide probes eliminates these problems.

Moving on from the original approach, a simpler system has been devised (Figure 2B), which obtains only thermal information and does not require Z-axis feedback. The high compliance of the probe allows scans of samples with large topographic variations. An X-Y stage controls the position of the probe while an interface circuit is used between the data acquisition computer and the thermal probe. A simple construction is enabled by eliminating Z-axis actuation and the hardware that is needed for it, such as photodetectors, lasers, and other electronics. An additional advantage is that the probes can be arrayed for high-throughput large-area scanning (Figure 1C).

Performance	Wollaston wire probe	Polyimide probe
Tip diameter	1 µm	<100 nm
Topographical resolution	NA	<1 nm
Temperature resolution	2.5 K	<10 mK
Thermal conductance	<0.23 µW K^{-1}	<3 pW K^{-1}
Normal spring constant	1-5 N m^{-1}	0.1 N m^{-1}

Table 1:
Comparison of characteristics of a Wollaston wire probe [7] and the polyimide thermal probe.

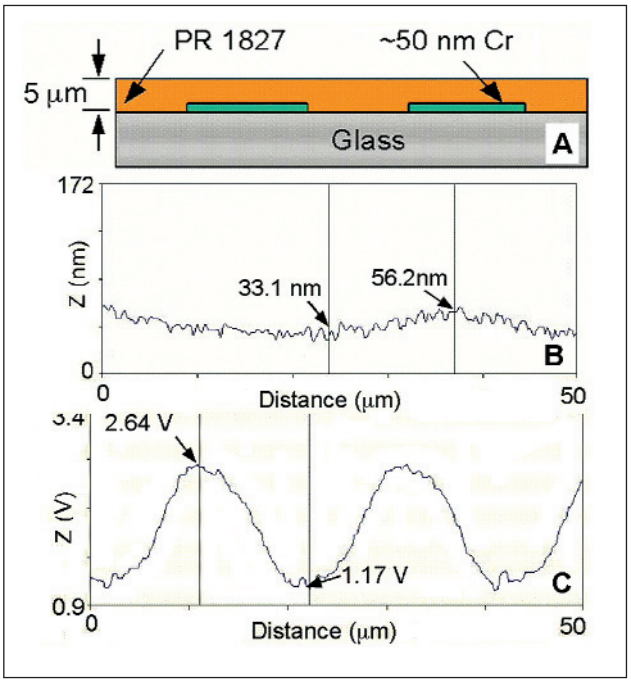

Figure 4:
(A) Schematic of a glass substrate with 50-nm thick Cr lines covered by 5 µm of photoresist.
(B) An AFM scan shows very little topographical variation.
(C) The Cr lines are clearly visible with a thermal probe scan. Reprinted from [15] with permission.

RESULTS AND DISCUSSION

SPM scans

Figure 3 contains scan images obtained without contact force feedback control using the system described above and depicted in Figure 2B. Scans of a developed Shipley UV-6 deep ultraviolet photoresist made without Z-direction feedback are shown in Figure 3A. The photoresist pattern was 350 nm thick and 500 nm wide. Comparing the line profiles with and without Z-direction feedback, the with-feedback operation provided higher signal-to-noise ratios. The fluctuation of the tip-sample contact area was larger without feedback. Figure 3B shows a thermal conductance map of developed polymethylmethacrylate (PMMA) on a four-inch silicon wafer. The photoresist pattern was 240-nm thick and 200-nm wide with a pitch of 400 nm. The scan results showed that the thermal probe can provide a spatial resolution better than 200 nm without contact-force feedback control [22].

Subsurface imaging capability is very useful for measuring semiconductor devices where multiple layers are present and the final IC is coated with a passivation layer. Thermal images showing metal lines through a passivation layer were obtained. Results demonstrating the subsurface imaging capability of the thermal probe are shown in Figure 4. A sample containing 50-nm thick chromium lines on a glass substrate was coated with a 5-µm thick planarized photoresist, which had a thermal resistivity of 0.193 W m^{-1} K^{-1} (Figure 4A). A topographical image of the sample showed that the photoresist was uniform and the underlying Cr layers were not detected (Figure 4B). The thermal image, on the other hand, clearly detected the underlying Cr layers. The variation in thermal resistance amounted to a 1% change in 1.0×10^{10} K W^{-1} and the signal-to-noise ratio was in excess of 15, as shown in Figure 4C [15].

Figure 5 illustrates another example of subsurface mapping. The sample contained 90-nm wide Cu lines covered with 250 to 300-nm wide and 125-nm thick natural oxide. An SEM picture of the trench before Cu deposition is shown in Figure 4A. An SEM picture of a Cu line is shown in Figure 5B. An AFM scan of the Cu lines covered with a thick layer of oxide is shown in Figure 5C. Figures 5D and 5E illustrate overlays of thermal scans superimposed on topographical scans and show <300 nm discontinuities in thermal conductance maps occurring under the natural oxide. These discontinuities were not visible topographically. The images revealed subsurface information about the Cu lines, which potentially may be related to Cu voids. The current through the probe was 12 mA and the nominal probe resistance was 26 Ω. The area scanned was 6×6 μm^2 and the scan rate was set at 1 Hz for Fig. 5D and 1.4 Hz for Fig. 5E.

Simulations

Numerical simulations were performed in order to demonstrate the feasibility of detecting voids in copper lines and to enhance understanding of the quality and detectability of the thermal conductance signal. Thermal scans over copper lines having various types of voids with different sizes and locations were simulated using the Femlab 3 Multiphysics Modeling package by Comsol [23]. Each simulation yielded maps of the change in thermal conductance as an area the size of the probe-tip heated the surface of the simulated copper lines.

The simulated structure was based on Intel's 130-nm process [24]. The structure consisted of a 400-nm thick lower layer of field oxide, the bottom of which was held at 0°C. The top layer was a dielectric, 280-nm thick, 1-µm wide, and 1-µm long, with a copper feature, 150-nm wide, 150-nm long, and 280-nm thick, located at the center of the dielectric. A void was simulated in the copper layer and its location and size were varied. A cylindrical thermal probe with 50-nm diameter resided on top of the copper and the probe temperature was held at 100°C at the point of contact with the copper.

Simulations of features with and without voids were performed and the heat flux out of the thermal probe was calculated. The number of bits of resolution in the sensed signal required in order to detect a particular void was determined from the difference in thermal resistance with and without a void for a particular depth. The simulations confirmed that voids in closer proximity to the surface and larger voids were easier to detect. The simulations also indicated that the minimum number of bits of resolution required to detect most voids was within the performance

levels of the scanning thermal microscopy system. For example, a 100-nm diameter void at 140-nm depth would require 8-bit resolution to be detected, while a 140-nm diameter void at the same depth would require 6 bits, and a 40-nm diameter void would require 12 bits. In Figure 6, the X axis represents the ratio of void depth to void diameter and the Y axis the bits required to detect a particular void. The two lines represent 70-nm and 140-nm depths. At a fixed depth, the bits required to detect a void decrease as the void size increases.

CONCLUSIONS

This article has reviewed a surface micromachined scanning thermal probe that uses polyimide as the structural material and an embedded thin-film metal resistor as the sensing element. The probe tip offers a diameter <100 nm, a topographical resolution of <1 nm, a spring constant of <0.1 N m^{-1}, and can be used to detect thermal conductance changes of the order of 3 pW K^{-1}.

The probe was used to map the spatial change in thermal conductance of various test samples. Surface and subsurface characteristics were observed. In particular, subsurface thermal conductance variations in copper lines have been observed. Past simulations have predicted the feasibility of copper-void detection by these probes. This work reports the first experimental demonstration of thermal conductance variations in copper lines using samples provided by Sematech.

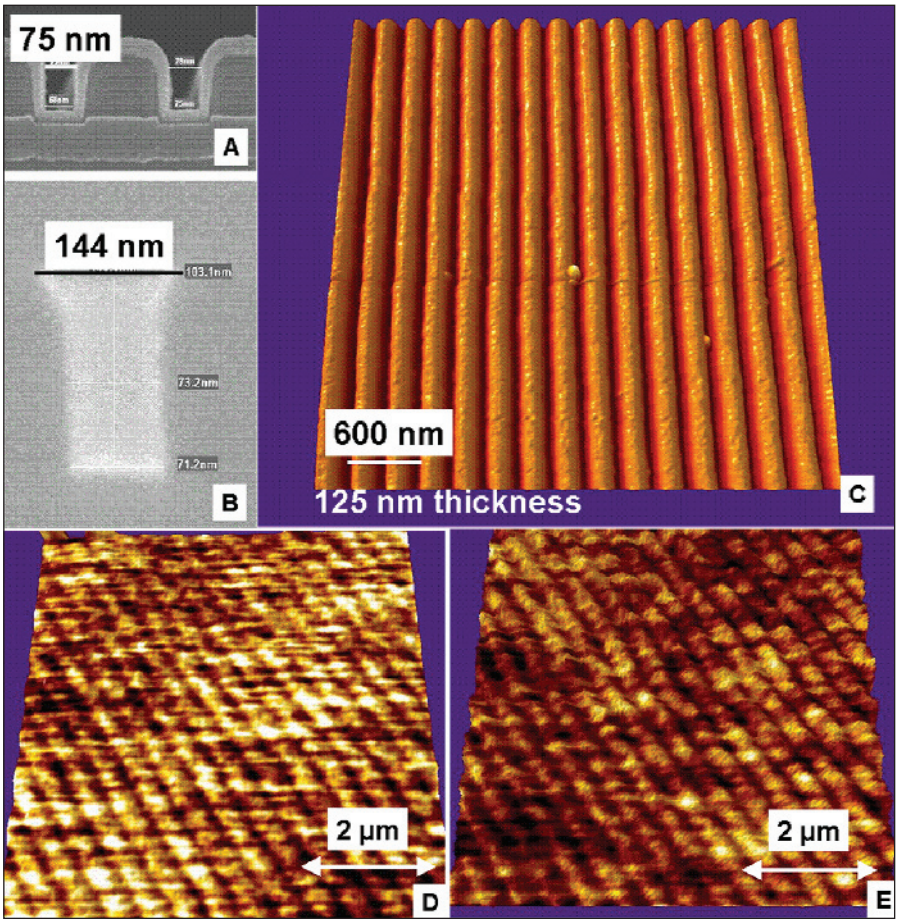

Figure 5:
(A) SEM image of cross-section of Cu line in 60-nm dense low-k dielectric film above porous low-k. Courtesy of Sematech.
(B) SEM image of trench preparation before Cu deposition. Courtesy of Sematech.
(C) AFM topographical image of Cu lines under a natural oxide 300-nm wide and 125-nm thick.
(D,E) Overlay thermal scans superimposed on topographical scans with <300 nm discontinuities in thermal conductance maps. These discontinuities occur under the natural oxide and are not visible topographically. The area scanned was 6 x 6 μm^2 and the scan rate was set at 1 Hz (D) or 1.4 Hz (E).

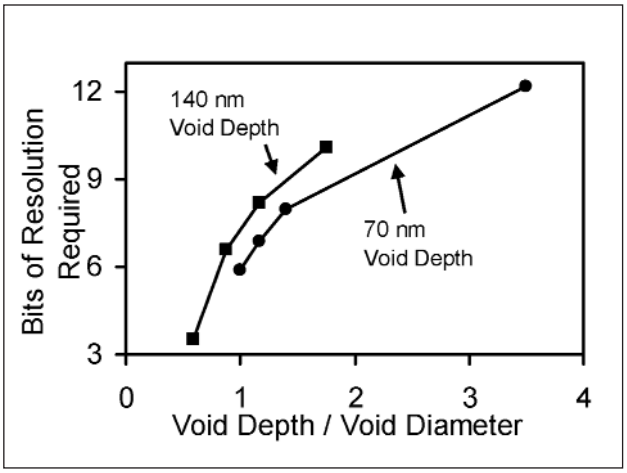

Figure 6:
The number of bits of resolution necessary to detect a void at a given depth is proportional to the ratio of the void depth to the void diameter. These simulations assume that the voids exist in a 150 nm x 150 nm x 280 nm feature of the copper, based on simulations reported in [23].

REFERENCES

1. Li, M-H., Gianchandani, Y. B. Sensors and Actuators A 104: 236–245, 2003.
2. Li, M-H. et al. IEEE/ASME Journal of Micro-electro-mechanical Systems 10(1):3-9, 2001.
3. Ocola, L. E. et al. J. Vac. Sci. Technol. B, 14(6):3974-3979, 1996.
4. Hammiche, A. et al. Meas. Sci. Technol., 7:142, 1996.
5. Luo, K. et al. Appl. Phys. Lett. 68:325, 1996.
6. Lai, J. et al. IEEE Electron Dev. Lett. 16:312, 1995.
7. ThermoMicroscopes, probe model #1615-00, now part of Veeco Probes, probe model #1615-00/1610-00/CLST-NOMB.
8. Hammiche, A. et al. Applied Spectroscopy 53(7):810-815, 1999.
9. Vettiger, P. et al. IBM J. Res. Develop. 44(3):323-340, 2000.
10. Lerchner, J. et al. Sensors and Actuators B 70:57-66, 2000.
11. Majumdar A. Scanning thermal microscopy. Ann. Rev. Mater. Sci. 29: 505-585, 1999.
12. Williams, C. C., Wickramasinghe, H. K. Appl. Phys. Lett.49:1587, 1986.
13. Gianchandani Y., Najafi, K. IEEE Transactions on Electron Devices 44(11):1857-1868, 1997.
14. Lee, J-H. et al. International Workshop on Thermal Investigations of ICs and Systems (THERMINIC 2002), Madrid, Spain, October 2002, pp. 111-116.
15. Lee, J-H., Gianchandani, Y. B. Review of Scientific Instruments 75(5):1222-1227, 2004.
16. Basu, A. S. et al. J. Vac. Sci. Technol. B, 22(6): 3217-3220, 2004.
17. Hendarto, E. et al. Proceedings 43rd Annual IEEE International Reliability Physics Symposium, pp. 294-299, 2005.
18. Basu, A. S., and Gianchandani, Y.B. Proceedings IEEE International Conference on MicroElectroMechanical Systems, Miami Beach, FL, pp 666-669, 2005.
19. Basu, A. S., Gianchandani, Y. B. Presented at the 13th International Conference on Solid-State Sensors, Actuators, and Microsystems, Seoul, Korea, 2005.
20. McNamara, S. et al. J. Micromech. Microeng. 15:237-243, 2005.
21. Gaitas, A., Gianchandani, Y. B. An experimental study of contact mode scan speed constraints for polyimide cantilever probes. To be published in Ultramicroscopy, 2006.
22. Li, M-H. Surface Micromachined Polyimide Scanning Thermocouple and Bolometer Probes. PhD Thesis, University of Wisconsin, Madison, January 2001.
23. McNamara, S., Gianchandani, Y. B. Systems and Methods for Thin Film Thermal Diagnostics with Scanning Thermal Microstructures. USA Provisional Patent, Application No. unassigned, Assignee: PicoCal Inc., Filed: September 2005.
24. Intel Technology Journal 6(2), May 16, 2002.

Available online at www.sciencedirect.com
SCIENCE DIRECT®
Sensors and Actuators A 104 (2003) 236–245
SENSORS AND ACTUATORS A PHYSICAL
www.elsevier.com/locate/sna

Applications of a low contact force polyimide shank bolometer probe for chemical and biological diagnostics

M.-H. Li, Y.B. Gianchandani*

Department of Electrical and Computer Engineering, Center for NanoTechnology, University of Wisconsin, Madison, WI, USA

Abstract

This paper reports on the detection of nano-scale chemical variations in photosensitive polymers and biological variations in cancerous tumor cells that have been accomplished for the first time using scanning thermal probes that we have developed. It also reports on changes that have been made over older versions of this probe to help achieve these capabilities. The probe is fabricated by a 6-mask surface micromachining process using polyimide as the structural material. A unique assembly sequence that involves flipping over the probe accommodates the future integration of circuitry on the same substrate. The probe has measured spring constant 0.082 N/m for a 250 μm × 50 μm × 3 μm probe. It offers a tip diameter of 50 nm. Probes are used to study exposed but undeveloped photoresist latent images in features of 70 nm, the acid diffusion in chemically amplified photoresist during post exposure bake, and HeLa cells. Lateral spatial resolution of <50 nm, topographic resolution of <1 nm and thermal resolution of <1.2 mK are demonstrated. Wet scanning capability, which widens the possibility of biochemical applications, is also demonstrated for the first time. The structure, fabrication, and assembly of the probe and the interface circuit used for these experiments are described.

Keywords: Polyimide shank; Bolometer; Chemical diagnostics

1. Introduction

Scanning thermal microscopy has been explored for a number of applications, including high resolution temperature mapping, topographical mapping, data storage, photothermal absorption spectroscopy, and subsurface imaging [1–4]. Temperature sensing methods used for scanning probes have included thermocouples, Schottky diodes, bolometers, and bimorphs [1–12]. A bolometer-type element which senses temperature by fractional changes in the electrical resistance provides certain advantages for microcalorimetry applications. In particular, this resistor can be used not only to sense temperature, but to supply heat if adequate current is passed through it. Since the tip temperature is ultimately influenced by the heat flow between the tip and the sample, variations in thermal conductance across the sample can be mapped by this probe. In essence, the device can be used as a spatially localized microcalorimeter [8,13].

We are developing ultra compliant thermal probes (with spring constant <0.1 N/m) for critical applications in ULSI lithography research. These include, specifically, mapping the latent image of exposed but undeveloped photoresist (PR) to measure photo-acid generation and diffusion independently from the developing step [14]. Since they offer sub-surface mapping capability, thermal probes also facilitate studies of intra-cellular features in bio-related research. To fulfill our need for these applications, probes must have a low spring constant to prevent damaging the soft materials, and provide spatial resolution <100 nm. In addition, to permit scanning in aqueous environments, complete electrical insulation is necessary. Wet scans are particularly challenging because of enhanced parasitic thermal losses, the need for complete electrical insulation, and the impact of surface tension on the ultra compliant probes. These requirements can not be fulfilled by using the commercially available wire probe which is made of bent bare wires, and has a high spring constant (5 N/m), limited spatial resolution, and no particular isolation [15].

We have previously reported thermocouple or bolometer probes fabricated by 6- to 7-mask surface micromachining processes using polyimide as the shank material, and the application of these probes for temperature mapping, subsurface imaging, and the measurement of glass transition temperature in photoresists [8,9]. This paper reports on applying these probes to ULSI lithography research,

* Corresponding author. Present address: 1301 Beal Avenue, UM Ann Arbor, MI 48109-2122, USA. Tel.: +1-734-615-6407.
E-mail address: yogesh@umich.edu (Y.B. Gianchandani).

0924-4247/03/$ – see front matter
doi:10.1016/S0924-4247(03)00026-8

particularly for mapping the latent image of exposed but undeveloped PR to measure photo-acid generation (PAG) and diffusion independently.[1] Wet scanning capability, which widens the possibility of biochemical applications, is also demonstrated for the first time. This paper also describes changes that have been made to older versions [8,9] of this probe to help achieve these capabilities. In the following text, Section 2 describes the device structure and fabrication process, Section 3 describes the measurement theory, and Section 4 describes experimental results that have been obtained.

2. Structure and fabrication

The basic structure of the probe is similar to that reported in [8,9], with a thin film bolometer sandwiched between two layers of polyimide, forming a cantilever. At one end of the cantilever the metal thin film protrudes through an opening in the lower polyimide layer, where it is molded into a pyramidal tip by a notch that was anisotropically wet-etched into the substrate. The tip and a portion of the probe shank are then released from the substrate by etching an underlying sacrificial layer. The released length is then folded over to extend past the die edge for clearance and held in place by an adhesive (Fig. 1). Typical dimensions of the probes after assembly are 250 μm length, 50 μm width, and 3 μm thickness with Cr/Au (200/2000 Å) for the tip and lead, which provides bolometer resistance of about 60 Ω. This flip-over method for providing the tip clearance exploits the mechanical flexibility of polyimide, and avoids the dissolution of the substrate material from underneath the tip. The polyimide shank offers both high mechanical compliance and high thermal isolation which are important for scanning soft samples with low thermal conductivity, such as PR and polymers.

The present manifestation of the probe (Fig. 2) has an additional thin evaporated film of gold (Cr/Au: 200/5000 Å) that serves as an AFM mirror and also permits a thermocompression bond to hold the probe after the flip-over step, eliminating the use of epoxy. This method retains the flatness of the probe and significantly increases yield. The released probe was manually flipped over, with the two gold pads (Fig. 2a) held together by using micromanipulators on a hot plate and slowly increasing hot plate temperature to 170 °C. The bonding strength is strong enough. No probe shank bounce back, cracking or breakage has been observed in the many 10s of samples that have been assembled in this manner. Other materials such as using partially curried photosensitive polyimide (PI2721™) or indium were also evaluated, but all show some drawbacks. The partially curried polyimide can be attacked by photoresist stripper, and the indium is attacked by the prolonged HF etching to release the probe tip. Other self-assembly approaches such as using surface tension forces [16] and a bimorph for stress mismatch were also studied, but all fail to retain the flatness of the flipped-over probe due to its fundamental limitation. Typical dimensions of the probes after assembly are 250 μm length, 50 μm width, and 3 μm thickness with Cr/Au (200/2000 Å) for the tip and lead, which have probe resistance about 60 Ω. The probe shank length can be easily adjusted by moving the location of the gold bond pads.

Another critical process step that has been added permits reduction of the tip diameter to about 50 nm by oxide sharpening the tip notch using the phenomena of the non-uniform

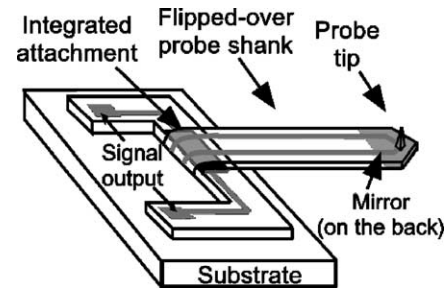

Fig. 1. Schematic of the ultracompliant polyimide thermal probe.

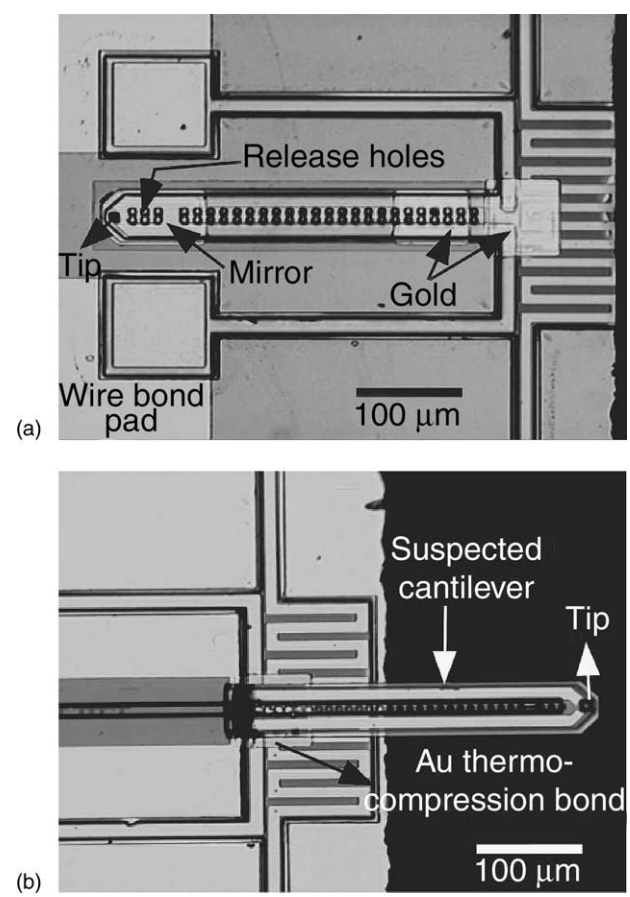

Fig. 2. (a) A scanning thermal probe showing the location of mirror and gold segments for thermocompression bond; (b) a 250 μm long probe flipped over the die edge and held down with a gold thermocompression bond.

[1] Portions of this paper will appear in [12].

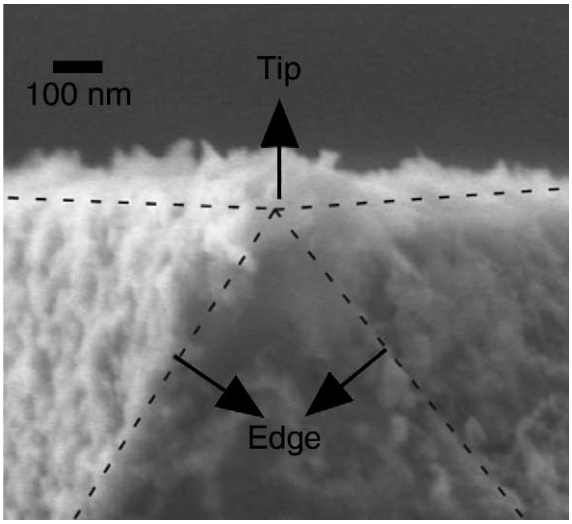

Fig. 3. Close-up of the sharpening tip showing the tip diameter is about 50 nm.

oxide growth [17]. A 4000 Å thick oxide is grown at 950 °C prior to depositing the sacrificial layer used for releasing the probe shank from the silicon substrate, which generates a tip diameter of about 50 nm as shown in Fig. 3.

Since the probe length is only about 300 μm, and the wafer thickness of a 3″ wafer is approximately 500 μm, a small extrusion at the die edge caused by the curvature of the dicing blade can block the laser beam (Fig. 4a). To provide a clear die edge for laser pickup, the probe wafer is bonded to a dummy wafer using photoresist, with the front side of the wafer covered by a thin photoresist film to protect the probes

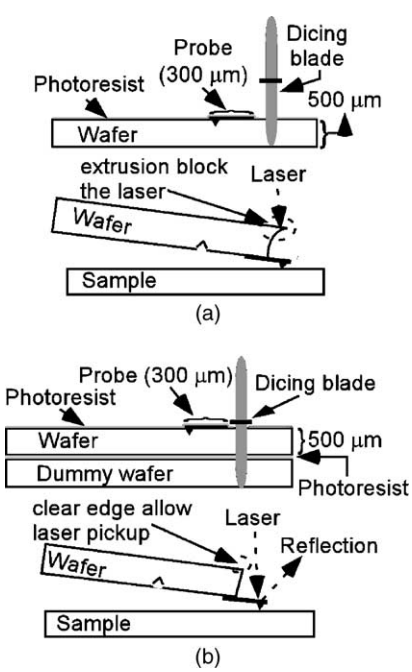

Fig. 4. (a) Extrusion at die edge blocks the laser; (b) with two wafers bonded and diced together to provide a clear die edge after dicing, which allows laser pickup.

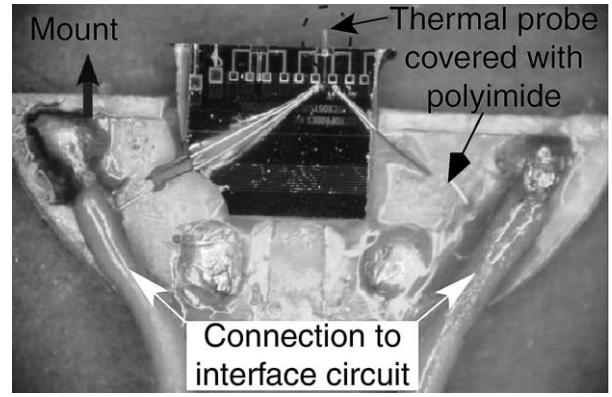

Fig. 5. A mounted scanning thermal probe with the base covered with a polyimide (PI2613^{TM}) layer to make it suitable for working in aqueous environments.

during dicing, and has both wafers diced together as shown in Fig. 4b. A 3″ wafer can generate about one thousand dies with two probes per die.

For operation in aqueous environments, the bond pads and bond wires are covered with a thin layer of polyimide (PI2613^{TM}), leaving the scanning tip as the only exposed metallic surface (Fig. 5). The polyimide probe provides high thermal probe shank resistance, low spring constant, and an integrated tip. These advantages make it suitable to study soft materials such as chemical amplified photoresist for deep-UV lithography and HeLa tumor cells.

3. Measurement theory

3.1. Interface circuit

Fig. 6 shows an interface circuit used to sense the probe resistance change as it scans across the sample surface. It includes a Wheatstone bridge, two gain stages providing combined amplification of 10^4, and a low-pass filter with a cutoff frequency of 1 kHz to reduce noise. The output voltage (V_{out}) is plotted for the thermal image.

When the probe resistance change (ΔR_P) is much smaller than the probe resistance (R_P), as in the case of thermal

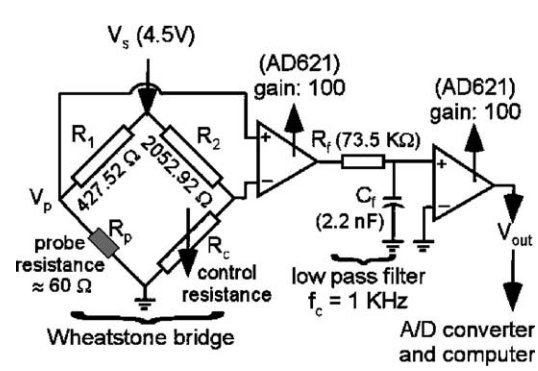

Fig. 6. An interface circuit for sensing the probe resistance change.

conductance contrast mapping, the output voltage change (ΔV_{out}) can be expressed as:

$$\Delta V_{out} \cong 10^4 \times V_s \times \Delta R_P \frac{R_1}{(R_1 + R_P)^2} \quad (1)$$

where V_s is the voltage applied to the Wheatstone bridge, and R_1 is a resistance of the Wheatstone bridge as shown in Fig. 6. The supplied power change (ΔP_p) of the probe resistor due to the probe resistance change (ΔR_P) is:

$$\Delta P_p \cong \frac{V_p^2}{R_P}\left(\frac{\Delta R_P(R_1 - R_P)}{R_P(R_1 + R_P)}\right) \quad (2)$$

According to Eqs. (1) and (2), the output voltage change (ΔV_{out}) is linearly proportional to the supplied power change (ΔP_p). Since the supplied power change (ΔP_p) is equal to the conductive heat loss between the tip and sample, which is proportional to change in the thermal conductance of the sample, the output voltage change (ΔV_{out}) represents the thermal conductance contrast of sample.

The probe tip temperature change (ΔT_P) can be calculated from the output voltage change (ΔV_{out}), which is:

$$\Delta T_P \cong \frac{\Delta V_{out}(R_1 + R_P)^2}{(10^4 V_s R_1 R_P \mathrm{TCR})} \quad (3)$$

The temperature coefficient of resistance (TCR) is 3640 ppm/K for Cr/Au (200/2000 Å) thin film. A ΔV_{out} of 100 mV corresponds to a ΔT_P of 5.657 mK calculated using the voltage and resistance values shown in Fig. 6. The full scale ΔT_P is indicated for all thermal scans presented in this paper. Before a scan, this circuit is adjusted to balance the Wheatstone bridge with the probe in contact with the sample by adjusting the control resistor (R_c) to make the resistance ratio of R_c/R_2 equal to R_P/R_1 so that the output voltage is as close as possible to 0 V in order to make full use of the available dynamic range.

3.2. Thermal conductance contrast mapping

When the probe is operated at a constant tip temperature (T_P), and with the sample thickness sufficiently thick compared with the tip diameter, the heat loss (P_s) to the sample can be expressed as [4]:

$$P_s = \frac{2\pi k_s a(T_P - T_0)}{1 + (2\pi k_s a R_g)} \quad (4)$$

The heat loss depends on the contact radius a, the ambient temperature T_0, and the tip-sample thermal contact resistance R_g, as well as the sample conductivity k_s. Assuming that the contact area and the tip-sample contact resistance do not change during a scan, the heat loss is then directly proportional to the sample thermal conductivity; i.e. for the image mapped to depend primarily on the sample thermal conductivity, it is necessary that $2\pi k_s a R_g \ll 1$. This requirement can be satisfied for a commercially available wire probe with tip diameter in the range of 1 μm when scanning samples with low thermal conductivity. For the polyimide probe, which has tip diameter ≈50 nm, this constraint is satisfied for virtually any case. Note that under this constraint the thermal probe can even be used to directly measure the sample thermal conductivity, since the supplied power will be directly proportional to it [18,19].

For the case of scanning an ultra-thin photoresist patterned on a silicon wafer with thickness comparable to the scan tip diameter, the heat transfer (P_s) between the probe tip and substrate can be modeled as heat flow through a cylinder:

$$P_s = \frac{(T_P - T_0)A_0 k_s}{H} \quad (5)$$

where T_P is the probe tip temperature, A_0 the tip-sample contact area, k_s the thermal conductivity of photoresist, and H the photoresist thickness. The silicon substrate is a large heat sink, effectively with a fixed temperature T_0. The thermal conductance image obtained from V_{out}, which depends on the heat flow (P_s), contains both topographic image and thermal conductivity information. To separate the influence of topographic variation from (V_{out}), both of the topographic and thermal images should be obtained simultaneously. The topographic image is produced by monitoring the deflection of the probe cantilever as in a conventional AFM by reflecting a laser beam from a mirror placed on the end of cantilever.

4. Measurement results

4.1. Spring constant and spatial resolution

The spring constant (k) is calculated by measuring the thermal fluctuations of the cantilever in the range of 5–25 kHz with the tip suspended 1 μm away from the sample surface using a built-in function in the Topometrix system [20–23]. The spring constant is given by:

$$k = \frac{a k_b T}{P_n} \quad (6)$$

where a is a correction factor (≈0.82), k_b the Boltzmann constant, T the ambient room temperature, and P_n the area of the power spectrum of the thermal fluctuations of the cantilever. The measured spring constant is 0.082 N/m for a 250 μm × 50 μm × 3 μm probe. Since the thermal fluctuations of the cantilever is measured by monitoring the tip motion using the optical-level method of an AFM, and only the fundamental mode of the thermal fluctuation of the cantilever is detected, the correction factor a is 0.82 [22,23]. If all the thermal fluctuation modes are detected, the value of the correction factor a will be 4/3. Another measurement is used to verify the linearity of the force-deflection response of the probe (Fig. 7). The force conversion is determined from the sensor response and the spring constant.

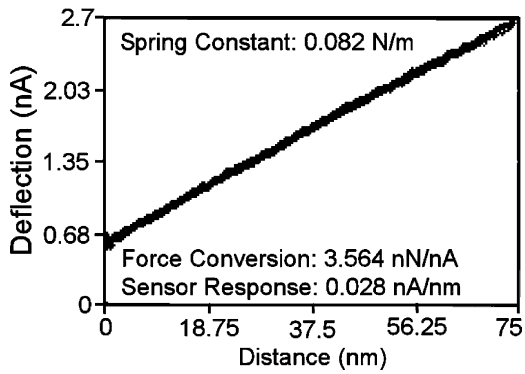

Fig. 7. The measured cantilever deflection versus the piezo displacement of a 250 μm × 50 μm × 3 μm probe. The cantilever deflection is represented in current, since it is determined by the photosensor response (PSPD).

Fig. 8 shows the scan results for same photoresist sample with z-direction feedback. The topographic image which uses the laser, and the thermal image which uses the resistor were obtained at the same time. The photoresist pattern is 350 nm thick, with trench of 500 nm wide in 2 μm pitch. The low spring constant allows scanning soft material such as photoresist pattern with feature size of 500 nm easily even without z-direction feedback (Fig. 9). The output voltage drops as the probe scanned across the higher thermal conductivity material (silicon), because the heat loss from the tip to sample increases, which cools down the

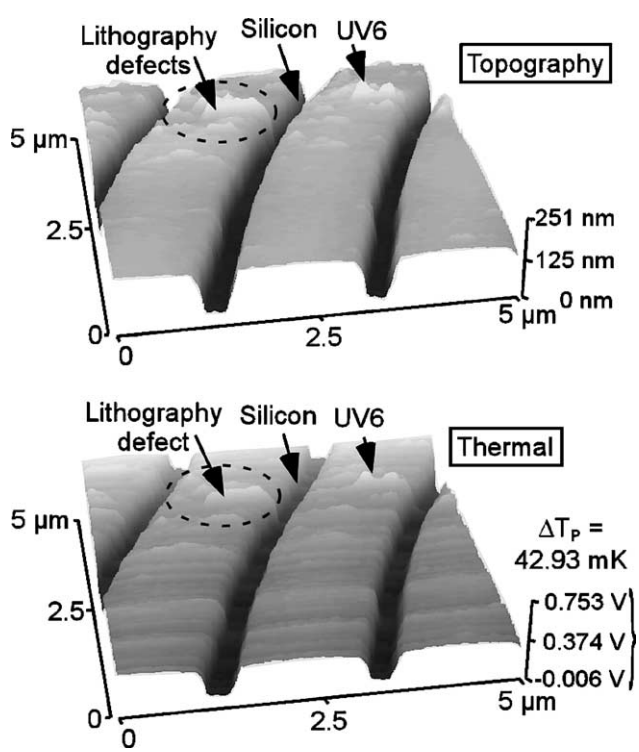

Fig. 8. Topographic (top) and thermal (bottom) images of developed UV6™ photoresist sample with thickness of 350 nm obtained with z-direction feedback.

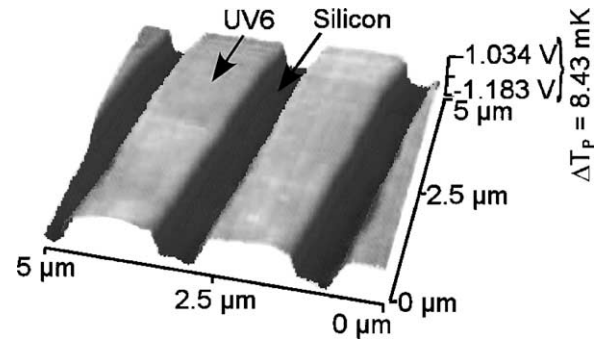

Fig. 9. Thermal image of the same photoresist sample of Fig. 8. No z-direction feedback.

tip temperature, and the corresponding probe resistance. It should be noted that in the absence of feedback control, topographic variations on the sample surface would cause variations in the tip-sample contact force which can potentially affect the image.

Fig. 10 shows the topographic and thermal images of exposed but undeveloped contact hole patterns in Shipley UV113™ photoresist patterned with critical dimension of 70 nm with 200 nm pitch. The images were obtained with scan rate of 0.75 μm/s and resolution of 400 lines. The thermal probe and interface circuit are sensitive enough to detect a photoresist thickness change only 4 nm, which corresponds to a tip temperature change as low as 1.13 mK. Comparing the topographic and thermal images of another photoresist sample shown in Fig. 11, the scan results clearly indicate the probe has spatial resolution of <50 nm, which is comparable to the smallest currently reported. The topographic resolution is <1 nm.

4.2. Photoresist chemistry

The positive tone chemically amplified photoresist UV6™ by Shipley, which is suitable for ultra-narrow linewidths ULSI lithography research, behaves as shown in Fig. 12 [24,25]. Unlike standard PR and PMMA, a photoacid generated by exposure permits catalyzed thermolysis of the backbone polymer during the post exposure bake (PEB), which changes the solubility of the exposed regions of the

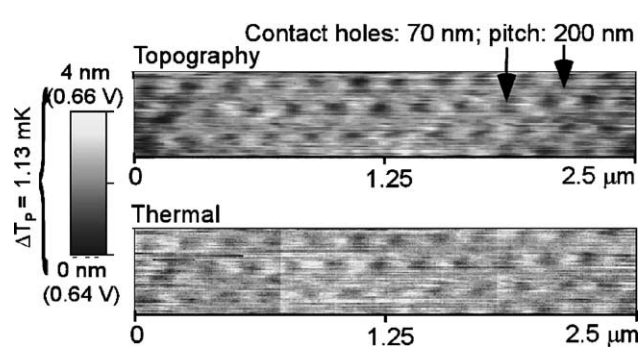

Fig. 10. Topographic (top) and thermal (bottom) images of exposed but undeveloped UV113™ photoresist contact holes of 70 nm.

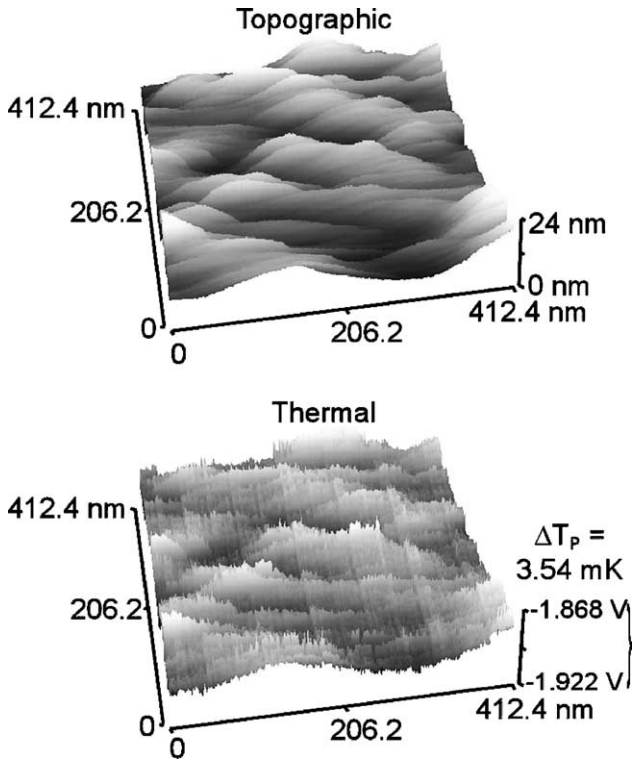

Fig. 11. Topographic (top) and thermal (bottom) images of partial developed UV113^{TM} photoresist sample show the thermal probe has spatial resolution of sub-50 nm.

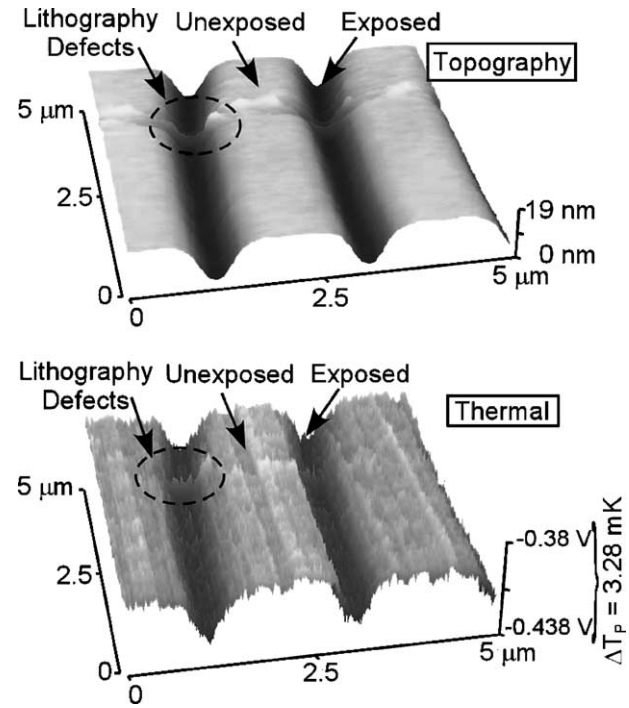

Fig. 13. Both of topographic and thermal images of exposed but undeveloped photoresist-UV6^{TM} of 500 nm thick on 4″ Si wafer obtained simultaneously. Sample was exposed by e-beam with charge density of 9 μC/cm^2, and then post exposure baked at 130 °C for 4 min.

resist and releases isobutylene. The photoresist thickness decreases in exposed areas where the released isobutylene is evaporated during PEB. Topographic variations and thermal conductance variations due to the thermolysis of the backbone are mapped simultaneously by using the thermal probe.

Fig. 13 shows the scan results of a 500 nm thick exposed but undeveloped UV6^{TM} on a 4″ silicon wafer. The sample was exposed using a Leica Cambridge 10.5 EBMF 30 kV electron beam lithography system with charge density of 9 μC/cm^2, and then post exposure baked at 130 °C for 4 min. As discussed previously, in chemically amplified photoresist, the

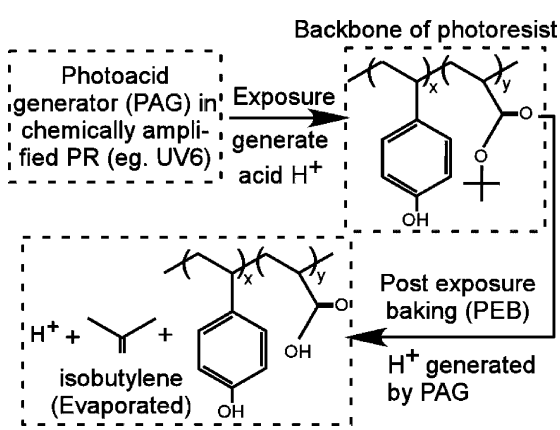

Fig. 12. The mechanism of chemically amplified photoresist UV6^{TM}. PAG acid deprotects the backbone during PEB for subsequent dissolution in the developer.

photoresist backbone is cleaved during PEB with an accompanying loss in free volume due to the releasing of isobutylene in the exposed area. The resulting change in thickness combined with the chemical change causes the output voltage to drop as shown in the thermal image. The ‘‘v’’ shape profile shown in the exposed area is due to the dose distribution of the e-beam source [14]. The small lithography defects shown both on the topographic and thermal images clearly indicate the high spatial resolution and sensitivity of thermal probe.

As discussed previously, a post exposure bake is usually required to activate the catalytic reactions. During PEB, acid generated by exposure diffuses and can cause pattern size changes [14,26,27]. It is therefore important to control the PEB conditions to suppress the acid diffusion for the critical dimension control of nanofabrication when using chemical amplification resist systems. Fig. 14 shows the topographic and thermal line scans of a trench in exposed but undeveloped Shipley UV6^{TM} photoresist with different duration of PEB times. As the duration of the 130 °C PEB increases from 45 to 360 s, both the topographic height change (Δh) and ΔV_{out} increase. However, the most significant change in Δh occurs in the 45–90 s period, whereas the most significant change in ΔV_{out} occurs in the 180–360 s period. As noted above, the Δh is due to the release of isobutylene and depends on the acid concentration and the reaction rate of photoresist backbone deprotection. The ‘‘v’’ shape profiles of exposed regions are due to the Gaussian distribution of the e-beam source of dose profile, and hence, the acid

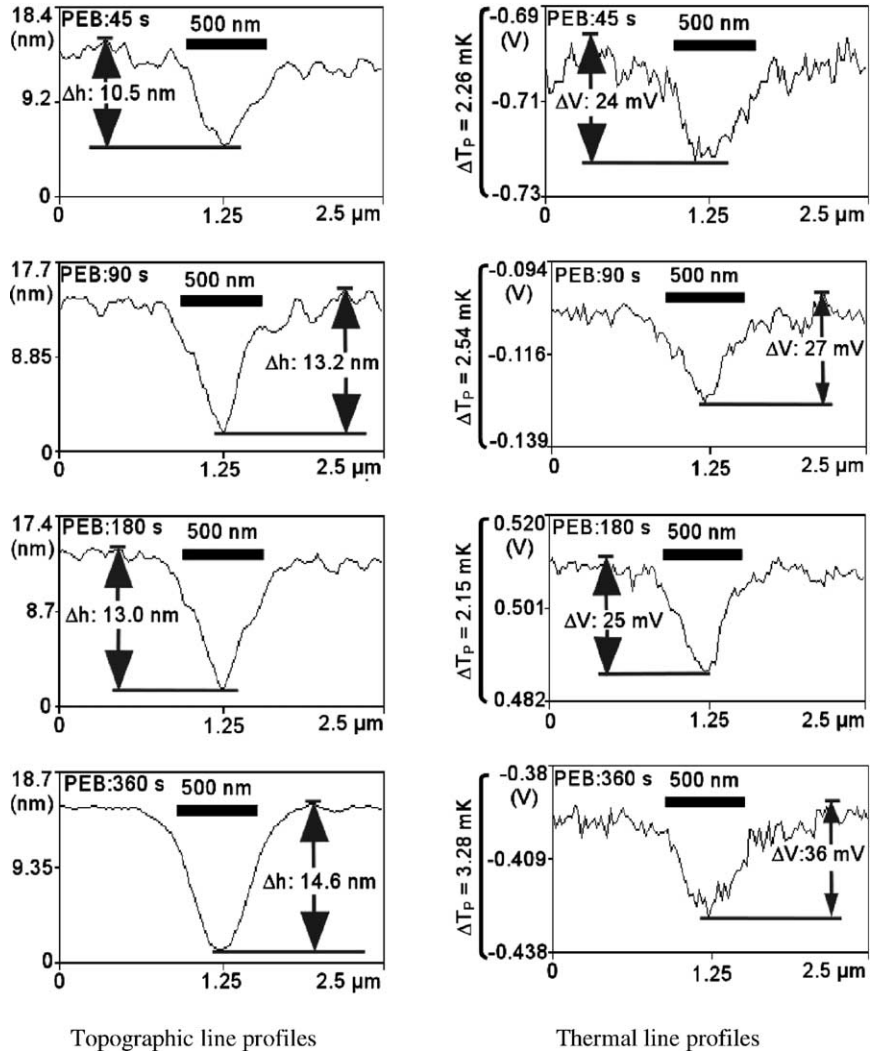

Fig. 14. Topographic (left) and thermal (right) line profiles across the exposed photoresist trench with sample of different post exposure bake time. Both of the topographic height change (Δh) and thermal voltage change (ΔV) increase as the PEB time increases.

concentration [14]. As the PEB time increases, the "v" shape profile widens due to the acid diffusion. However, since the acid diffusion constant, which depends on the process conditions [28], is only about of 50 nm^2/s for UV6™ [26], this change is very small (~10 nm) [29], particularly when compared to the 500 nm width of the exposed portion. Since the recommended PEB condition for 130 °C is 90 s, the longer PEB times may deplete the photoresist backbone, minimizing subsequent changes in topography. In contrast, other chemical changes may lead to the ΔV_{out} increase during the 180–360 s period.

4.3. Biological analysis

A eukaryotic cell contains many membrane-limited compartments knows as organelles (mitochondrion, lysosome, etc.) separated by the cytoplasm, and a nucleus bounded by a double membrane. The organelles have different cellular functions, and have slightly different thermal conductivity compared with that of cytoplasm. In addition, the temperatures of some organelles are expected to be different. For example, the mitochondria are the energy generators of the cell. Therefore, the temperature at the mitochondria should be higher. The thermal probes are capable of mapping both thermal conductance and temperature variations. Since subsurface variations in these quantities can be detected while the topography is being mapped as well, the thermal probes can potentially be useful tools for studying cellular activity under different conditions. The low spring constant (0.082 N/m), the high thermal isolation, and high spatial resolution (<50 nm) of the polyimide probes are important assets in this kind of application. Here, we demonstrated the usage of applying the thermal probe to map the thermal conductance contrast of fixed HeLa tumor cells, which are widely used for studying cellular functions [30]. These cells typically have a diameter of about 30 μm, with a very large nucleus. The optical, topographic and thermal images of the nucleus of a HeLa cell fixed to a glass slide while undergoing

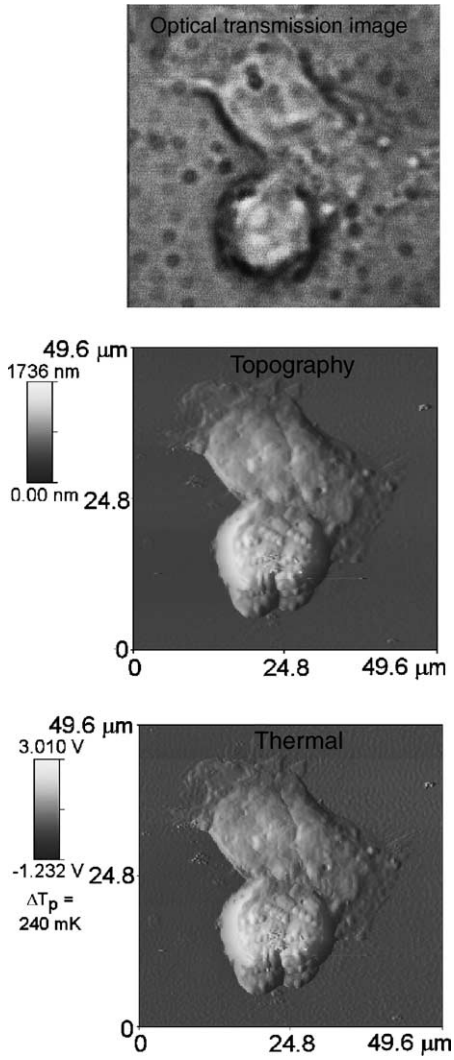

Fig. 15. The optical, topographic and thermal images of the nucleus of a HeLa cell fixed to a glass slide while undergoing mitosis. The optical image was obtained from transmission microscopy. The topographic and thermal images obtained from thermal probes are almost identical since the probe tip heat loss due to topographic change is dominant.

mitosis are compared in Fig. 15. The optical image was obtained using transmission microscope (Axiovert 100TV) with samples in the microscope immersion oil. Since the topographic variation in such a sample is much larger than the thermal conductivity difference of the organelles within it, the thermal image is expected to be similar to the topography map. The distinctions between these images are evidence of variations in subsurface conductivity.

4.4. Scanning in aqueous environments

Aqueous scans are particularly challenging because of enhanced parasitic thermal losses between the probe shank and substrate, the need for complete electrical insulation, and the impact of surface tension on the ultra compliant probes. The probe and mounting platform must be immersed in the liquid along with the sample to circumvent the surface

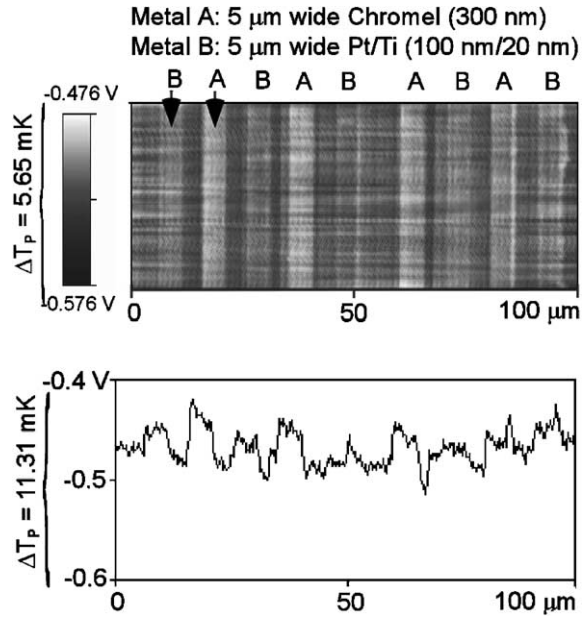

Fig. 16. Area (upper) and line scan (lower) thermal images of metal stripes on a Si substrate obtained without z-direction feedback with the probe and sample immersed in water.

tension forces, and to provide a uniform surrounding environment. The spatial resolution and temperature sensitivity degrade due to the parasitic thermal liquid conductance between the probe shank and sample. Since the liquid (~1 W/m K) has much higher thermal conductivity than that of air (2.6×10^{-2} W/m K), the heat transfer between the probe shank and sample substrate can no longer be neglected.

Fig. 16 presents area and linear thermal scans of metal lines on a Si substrate in an aqueous environment. The sample was 5 μm wide thin film chromel (metal A: 300 nm thick), and Ti/Pt (metal B: 20/100 nm thick) patterned on a Si substrate and isolated from it by a 0.75 μm thick silicon dioxide layer. The variation in metal films is clearly detectable despite the fact that these scans were performed without *z*-axis feedback. This is possible because of the ultra compliant nature and high thermal isolation offered by the probe. We believe this is the first scanning thermal probe that can work in aqueous environment. With the ability of scanning in aqueous environments, these probes can potentially facilitate studies of cellular features and functions of living cells in real time to provide other information not provided by AFM, such as the temperature distribution in a cell that is undergoing mitosis.

4.5. Performance analysis

Table 1 shows the current performance of polyimide thermal probe with the interface circuit. The probe has tip diameter about 50 nm, and spatial resolution of sub-50 nm as shown in Figs. 4 and 11 respectively. According to Fig. 14, the thermal probe can easily detect output voltage changes

Table 1
Current performance of polyimide thermal probe with the interface circuit

Tip diameter (nm)	≈50
Lateral spatial resolution (nm)	<50
Topographic resolution (nm)	<1
Input referred circuit noise (1 kHz BW) (μV)	<2
ΔR resolution (mΩ)	<0.25
Tip temperature resolution (mK)	<1.2
Detectable thermal conductance change (W/K) (1%)	1×10^{-11}
Detectable thermal conductivity change (W/m K) (1%)	2×10^{-3}

lower than 20 mV. Since interface circuit has voltage gain of 10^4, this indicates the interface circuit can detect input signal change lower than 2 μV. Calculated using Eqs. (1) and (3), this also indicates the interface circuit can sense 0.25 mΩ probe resistance change or 1.2 mK temperature change in the probe temperature.

Comparing the line profiles of topographic and thermal scan at unexposed area in Fig. 13, it shows the thermal probe can easy detect photoresist thickness change lower than 1% (5 variation of 500 nm thick). Since the output voltage is proportional to the thermal conductance between the tip and silicon substrate, which is $k_s A_0/H$ as discussed at Eq. (5), it implies the thermal probe can also detect thermal conductance change lower than 1%, which is 1.09×10^{-11} W/K (1% of $k_s A_0/H$) by assuming that the tip-sample contact area (A_0) is $30^2\ \pi$ nm^2, and the thermal conductivity of photoresist (k_s) is comparable to that of PMMA (0.193 W/m K) [2]. By the same argument, the thermal probe can also detect the thermal conductivity changes lower than 1%, which is 1.93×10^{-3} W/m K.

5. Conclusion

This effort has addressed the development and applications of a polyimide shank thermal probe fabricated by a 6-mask surface micromachining. These probes are assembled with the help of a thermocompression bond between thin films that greatly improved yield. A modification of the structure permits operation in aqueous environments. Typical probe dimensions are 250 μm length, 50 μm width, and 3 μm thickness. The probe is ultra-compliant with a spring constant of 0.082 N/m, and can be further reduced by reducing the probe width and thickness. It can be operated without z-direction feedback, even when scanning soft materials.

The probe has a lateral spatial resolution of sub-50 nm, and a topographical resolution of <1 nm. Combined with the interface circuit, the probe can offer tip temperature resolution better than 1.2 mK. The probe has been used to scan exposed but undeveloped photoresist samples, HeLa cells, and to study the acid diffusion in photoresist during post exposure bake. A sample scanned with both of probe and sample immersed in water is also presented. These results suggest the potential usefulness of the polyimide probe as a tool for measuring the cellular activity of living cells in aqueous environments.

Acknowledgements

The authors thank Prof. Cerrina and Dr. Leo Ocola for supporting the photoresist samples, and Prof. Menon and Dr. Vainauskas for providing HeLa cell samples. This work was funded in part by the Semiconductor Research Corporation contract # 98-LP-452.005. The Center for NanoTechnology, University of Wisconsin-Madison, is supported in part by DARPA/ONR grant # MDA 972-00-1-0018, and # MDA 972-99-1-0013. The Synchrotron Radiation Center, University of Wisconsin-Madison, at which some of the experimental facilities are located, is operated under NSF award # DMR-0084402.

References

[1] H.K. Wickramasinghe, Scanned-Probe Microscopes, Scientific American, 1989, pp. 98–105.
[2] A. Hammiche, D.J. Hourston, H.M. Pollock, M. Reading, M. Song, Scanning thermal microscopy: subsurface imaging, thermal mapping of polymer blends, and localized calorimetry, J. Vac. Sci. Technol. B 14 (2) (1996) 1486–1491.
[3] P. Vettiger, M. Despont, U. Drechsler, U. Dürig, W. Häberle, M.I. Lutwyche, H.E. Rothuizen, R. Stutz, R. Widmer, G.K. Binnig, The millipede-more than one thousand tips for future AFM data storage, IBM J. Res. Develop. 44 (3) (2000) 323–340.
[4] A. Majumdar, Scanning thermal microscopy, Annu. Rev. Mater. Sci. 29 (1999) 505–585.
[5] Y. Suzuki, Novel microcantilever for scanning thermal imaging microscopy, Jpn. J. Appl. Phys. Part 2 35 (3A) (1996) L352–L354.
[6] Y.B. Gianchandani, K. Najafi, A silicon micromachined scanning thermal profiler with integrated elements for sensing and actuation, IEEE Trans. Electron Dev. 44 (11) (1997) 1857–1867.
[7] T. Leinhos, M. Stopka, E. Oesterschulze, Micromachined fabrication of Si cantilevers with Schottky diodes integrated in the tip, Appl. Phys. A 66 (1998) S65–S69.
[8] M.-H. Li, Y.B. Gianchandani, Microcalorimetry applications of a surface micromachined bolometer-type thermal probe, J. Vac. Sci. Technol. B 18 (6) (2000) 3600–3603.
[9] M.-H. Li, J.J. Wu, Y.B. Gianchandani, Surface micromachined polyimide scanning thermocouple probes, J. Microelectromech. Syst. 10 (1) (2001) 3–9.
[10] D.-W. Lee, T. Ono, T. Abe, M. Esashi, Fabrication of microprobe array with sub-100 nm nano-heater for nanometric thermal imaging and data storage, in: Proceedings of the 11th International Conference On Solid-State Sensors and Actuators (Transducers '01), June 2001, pp. 204–207.
[11] L. Shi, O. Kwon, A.C. Miner, A. Majumdar, Design and batch fabrication of probes for sub-100 nm scanning thermal microscopy, J. Microelectromech. Syst. 10 (3) (2001) 370–378.
[12] M.-H. Li, J.-H. Lee, F. Cerrina, A.K. Menon, Y.B. Gianchandani, Chemical and biological diagnostics using fully insulated ultra-compliant thermal probes, in: Proceedings of the Hilton Head 2002, Solid-State Sensor, Actuator, and Microsystems Workshop, 2–6 June 2002.
[13] D. Fryer, P. Nealey, J. de Pablo, Thermal probe measurements of the glass transition temperature for ultrathin polymer films as a function of thickness, Macromolecules 33 (17) (2000) 6439–6447.

[14] L.E. Ocola, D. Fryer, P. Nealey, J. dePablo, F. Cerrina, S. Kämmer, Latent image formation: nano-scale topography and calorimetric measurements in chemical amplified resists, J. Vac. Sci. Technol. B 14 (6) (1996) 3974–3999.
[15] TM Microscopes, http://www.tmmicro.com, Probe Model no. 1615-00.
[16] R.R.A. Syms, Equilibrium of hinged and hingeless structures rotated using surface tension forces, J. Microelectromech. Syst. 4 (4) (1995) 177–184.
[17] S. Akamine, C.F. Quate, Low temperature thermal oxidation sharpening of microcast tips, J. Vac. Sci. Technol. B 10 (5) (1992) 2307–2310.
[18] F. Ruiz, W.D. Sun, F.H. Pollak, C. Venkatraman, Determination of the thermal conductivity of diamond-like nanocomposite films using a scanning thermal microscope, Appl. Phys. Lett. 73 (13) (1998) 1802–1804.
[19] D.I. Florescu, V.M. Asnin, F.H. Pollak, A.M. Jones, J.C. Ramer, M.J. Schurman, I. Ferguson, Thermal conductivity of fully and partially coalesced lateral epitaxial overgrown GaN/sapphire (0001) by scanning thermal microscopy, Appl. Phys. Lett. 77 (10) (2000) 1464–1466.
[20] J.L. Hutter, J. Bechhoefer, Calibration of atomic-force microscope tips, Rev. Sci. Instrum. 64 (7) (1993) 1868–1873.
[21] Topometrix Corporation, User's Manual Supplement, SPMLab Version 3.06, 1995, pp. 2–19s.
[22] J. Bechhoefer, J.L. Hutter, unpublished.
[23] H.-J. Butt, M. Jaschke, Calculation of thermal noise in atomic-force microscopy, Nanotechnology 6 (1995) 1–7.
[24] R.D. Allen, W.E. Conley, R.R. Kunz, Deep-UV resist technology, in: P. Rai-Choudhury (Ed.), Handbook of Microlithography, Micromachining and Microfabrication, vol. 1, Microlithography, SPIE, Bellingham, Washington, 1997.
[25] H. Ito, Chemically amplified resists: past, present, and future, SPIE 3678 (1999) 2–12.
[26] D. Kang, E.K. Pavelchek, C. Swible-Keane, The accuracy of current model descriptions of a DUV photoresist, SPIE 3678 (1999) 877–890.
[27] T. Yoshimura, T. Nakayama, S. Okazaki, Acid-diffusion effect on nanofabrication in chemical amplification resist, J. Vac. Sci. Technol. B 10 (6) (1992) 2615–2619.
[28] T. Itani, H. Yoshino, S. Hashimoto, M. Yamana, N. Samoto, K. Kasama, A study of acid diffusion in chemically amplified deep ultraviolet resist, J. Vac. Sci. Technol. B 14 (6) (1996) 4226–4228.
[29] T.H. Fedynyshyn, J.W. Thackeray, J.H. Georger, M.D. Denison, Effect of acid diffusion on performance in positive deep ultraviolet resists, J. Vac. Sci. Technol. B 12 (6) (1994) 3888–3894.
[30] R.L. Warters, O.L. Stone, Histone protein and DNA synthesis in HeLa cells after thermal shock, J. Cell. Phys. 118 (1984) 153–160.

巴工業株式会社

化学品本部機能材料部第一課

〒141-0032 東京都品川区大崎1-2-2 アートヴィレッジ大崎セントラルタワー
Tel: 03-5435-6515 Fax: 03-5435-0071
Web-site: http://www.tomo-e.co.jp E-mail: akobayashi@tomo-e.co.jp
nanotech@tomo-e.co.jp